

Bayesian Robust Learning in Chain Graph Models for Integrative Pharmacogenomics

Moumita Chakraborty¹, Veerabhadran Baladandayuthapani², Anindya Bhadra³, and Min Jin Ha^{*1}

¹Department of Biostatistics, The University of Texas MD Anderson Cancer Center, Houston, TX

²Department of Biostatistics, University of Michigan, Ann Arbor, MI

³Department of Statistics, Purdue University, West Lafayette, IN

Abstract

Integrative analysis of multi-level pharmacogenomic data for modeling dependencies across various biological domains is crucial for developing genomic-testing based treatments. Chain graphs characterize conditional dependence structures of such multi-level data where variables are naturally partitioned into multiple ordered layers, consisting of both directed and undirected edges. Existing literature mostly focus on Gaussian chain graphs, which are ill-suited for non-normal distributions with heavy-tailed marginals, potentially leading to inaccurate inferences. We propose a Bayesian robust chain graph model (RCGM) based on random transformations of marginals using Gaussian scale mixtures to account for node-level non-normality in continuous multivariate data. This flexible modeling strategy facilitates identification of conditional sign dependencies among non-normal nodes while still being able to infer conditional dependencies among normal nodes. In simulations, we demonstrate that RCGM outperforms existing Gaussian chain graph inference methods in data generated from various non-normal mechanisms. We apply our method to genomic, transcriptomic and proteomic data to understand underlying biological processes holistically for drug response and resistance in lung cancer cell lines. Our analysis reveals inter- and intra- platform dependencies of key signaling pathways to monotherapies of icotinib, erlotinib and osimertinib among other drugs, along with shared patterns of molecular mechanisms behind drug actions.

Keywords: Bayesian graphical models; Cancer; Data integration; Robust graphical models; Multi-platform genomics; Pharmacogenomics.

*Email: MJHa@mdanderson.org

1 Introduction

Pharmacogenomics encapsulates genomic mechanisms governing variable drug response and has been implemented into drug development pipeline to improve drug effectiveness and to reduce adverse drug reactions and toxicity (Squassina et al., 2010; Roden et al., 2019). In cancer, utilizing the underlying genomic profile of tumors, especially the downstream effects of genes and their products for better understanding drug mechanisms, can lead to the development of more effective and robust treatment regimes (Kasarskis et al., 2011). In non-small cell lung cancer (NSCLC) patients, for example, clinical trials have shown that the epidermal growth factor receptor (EGFR) T790M mutation confers resistance to first-generation tyrosine kinase inhibitors (TKIs), which has led to the development of new EGFR inhibitors such as osimertinib that show efficacy superior to that of standard EGFR-TKIs (Mok et al., 2017; Soria et al., 2018). Patients with atypical EGFR mutations, on the other hand, show heterogeneous and reduced responses to EGFR inhibitors including osimertinib, and there are currently no established guidelines for the uncommon mutations (Robichaux et al., 2021). The basic underlying premise is that accounting for the heterogeneity in drug sensitivity in relation to multiple molecular domains, while utilizing preclinical models of human cancer, is a key step toward discovering holistic functional mechanisms of anticancer drugs, which could facilitate better systems for classifying tumor and more robust clinical trial designs (Bedard et al., 2013; Lim and Ma, 2019).

These efforts have been catalyzed through consortium-level efforts such as the Cancer Dependency Map (The DepMap Portal; www.depmap.org), which provides a rich data repository for human cancer cell lines that encompass various types of primary cancers for identifying targetable genes and their functional relations across diverse domains of biological information. The portal includes multi-platform data such as copy number alteration (CNA), mRNA expression, and reverse phase protein array (RPPA) based protein expres-

sion obtained from the Cancer Cell Line Encyclopedia (CCLE) (Ghandi et al., 2019). It also contains drug sensitivity outcomes of more than 4,000 drugs for these CCLE samples, which are based on high-throughput growth-inhibitory drug activities screened using Profiling Relative Inhibition Simultaneously in Mixtures (PRISM) technology (Corsello et al., 2020). Most existing pharmacogenomic analyses are limited to identifying the association of molecular features with drug sensitivity without characterization of within- and cross-platform dependencies (Iorio et al., 2016; Corsello et al., 2020). A unified framework that provides a detailed characterization of multi-platform regulatory behavior can help in identifying key biological mechanisms of drug action to facilitate drug development.

To this end, we employ a graph-theoretic approach that captures dependencies among biological variables, where a node represents information on each unit and an edge between two nodes is an indicator of interaction or dependence between the corresponding biological units. For multi omic data, we assume that the entire set of nodes is partitioned into multiple platforms that are ordered based on fundamental biological principles. The platforms corresponding to datasets in our study are assumed to be ordered as: $\{\text{CNA} \rightarrow \text{mRNA} \rightarrow \text{RPPA} \rightarrow \text{Drugs}\}$, so that platforms lower in the hierarchy regulate data in higher platforms (Morris and Baladandayuthapani, 2017). This conceptual structure of our data is explained through Figure 1a, which can be cast as a *chain graph* structure, where the set of nodes can be naturally partitioned into disjoint subsets, called layers with a pre-established order induced by biology. Edges between nodes within a layer are undirected and those between layers are directed, pointing towards the layer placed higher in the hierarchy.

Joint modeling of the mixed dependency structure in a chain graph, containing hierarchical multiple sub-graphs with directed and undirected edges, engenders substantial methodological and technical challenges. Most existing approaches rely on Gaussian assumptions on chain graphs, that simplify the methodological and computational complexities. Two-layer Gaussian chain graph models (GCMs) have been studied in the frame-

work of multivariate Gaussian regressions or covariate adjusted Gaussian graphical models (Rothman et al., 2010; Yin and Li, 2011; Bhadra and Mallick, 2013; Chen et al., 2016; Li et al., 2021). GCMs with more than two layers have been considered by Lin et al. (2016) through penalized maximum likelihood estimation of the coefficients and the precision matrix, and Ha et al. (2021) who proposed a Bayesian approach to coherently learn chain graphs by variable selection on node-wise conditional likelihoods. More multi-layered GCM estimation methods can be found in Drton and Eichler (2006), Drton and Perlman (2008), McCarter and Kim (2014), and Petersen (2018) among others.

Although GCMs have been used (successfully) for a broad range of biological data that are continuous (or transformed to be continuous), they are ill-suited when the underlying variables exhibit considerable non-normal characteristics such as skewness, heavy tails and multimodal marginal distributions. As a motivating example, Figure 1b,c display the empirical density and normal quantile-quantile (Q-Q) plot respectively, of CNA levels of MAPK1, a gene controlling several cell signaling processes such as proliferation and transcriptional regulation in different cancers (Vicent et al., 2004), across the 104 lung cancer cell lines in our case study (detailed in Section 5). There is clear evidence of a heavier-than-normal tail due to extreme values observed in the right tail. We further quantify the “degree of non-normality” for all nodes across the four layers, based on the score: $H(\mathbf{x}) = 2 * \Phi(\log(1 - pval(\mathbf{x})))$, where Φ is the cdf of standard normal distribution, and $pval(\mathbf{x})$ is the p -value of the Kolmogorov-Smirnov test for normality of \mathbf{x} . The H -score is between 0 and 1 with the higher value indicating the higher departure from normality. CNA and drug nodes show significant levels of non-normalities. Moreover, high levels of within-layer H -score variations are detected, which implies node-specific tail behavior.

Modeling background and the current state of the art. Modeling non-normality in multivariate data has been performed using copulas (e.g., Nelsen, 2007; Genest and Nešlehová, 2014). Gaussian copula models that use a set of latent variables following a

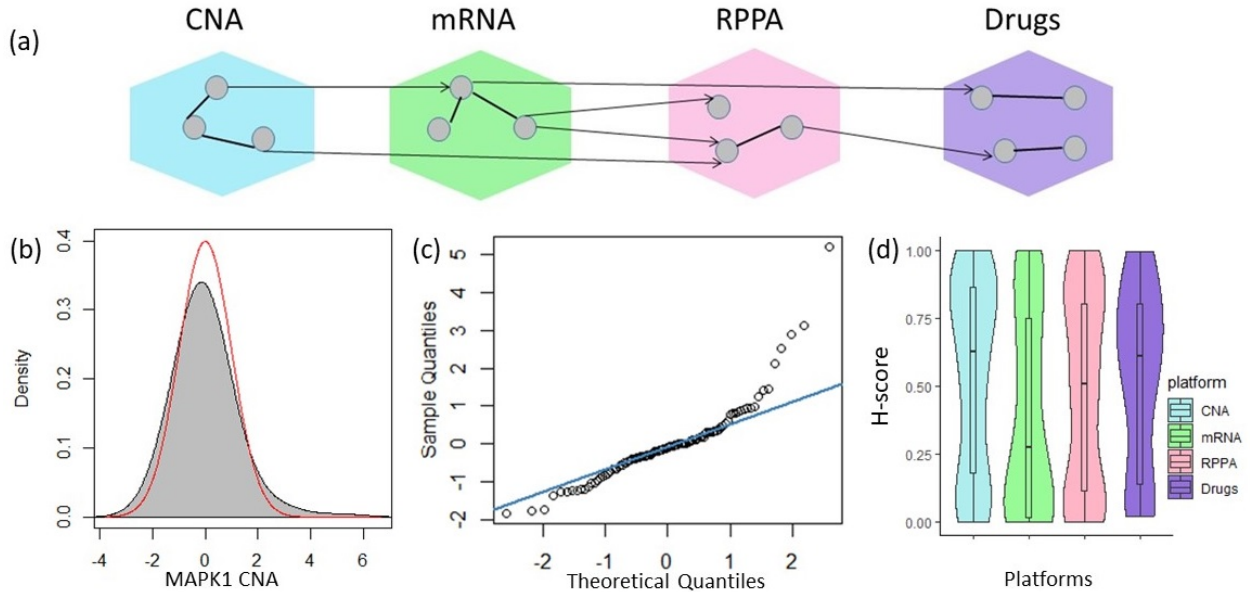


Figure 1: (a) Chain graph structure for CNA, mRNA, RPPA and drug layers, with directed and undirected edges between nodes of different and same layers respectively. (b) Empirical density plot of MAPK1 CNA levels. The H -score defined in the text as a measure of non-normality is equal to 0.988 for MAPK1 CNA. The red curve is the density of standard normal distribution. (c) Normal q-q plot of data corresponding to MAPK1 CNA levels (d) H -scores across multi-platform genomic data and 20 drugs.

multivariate normal distribution, have been discussed by (Pitt et al., 2006; Dobra et al., 2011). Liu et al. (2009) provide a semiparametric non-paranormal model and show that it is equivalent to a Gaussian copula when all the variables are continuous. Estimation methods for the non-paranormal model have been developed using various rank-based measures of dependence (Liu et al., 2012; Xue and Zou, 2012). These methods assume the transformation of the original variables into latent Gaussian variables to be deterministic. Relatively fewer works have focused on dependencies among variables under a random transformation.

In networks with non-normal continuous marginals with random transformations leading to Gaussian latent variables, early Bayesian works include Finegold and Drton (2011) and Finegold and Drton (2014), who modeled the node marginals using the multivariate- t or Dirichlet- t distributions. The multivariate- t model of Finegold and Drton (2011) that assumes the same scaling transformation for each node can infer dependencies on the orig-

inal variables through *conditional uncorrelatedness*. This model is, however, less flexible than their alternative- t model and the Dirichlet- t that allow different node-wise scaling factors. To infer dependencies on the original scale of data using a more flexible model such as Dirichlet- t , Bhadra et al. (2018) proposed a Bayesian framework based on random scale transformations that helps in modeling skewed and heavy-tailed continuous marginals while allowing each node to have a different marginal distribution modeled in a data-dependent manner. Moreover, Bhadra et al. (2018) introduced the property of *conditional sign independence*, which is weaker than conditional independence, but holds among *observed variables* under non-normal marginals; we reserve formal definitions for Section 2. None of the above mentioned methods however, are applicable to chain graphs. We build on the approach of random scale-transformations in the context of non-Gaussian chain graphs, by allowing appropriately scaled transformations of node-marginals to be normally distributed, with the additional flexibility of inferring conditional (in)dependence on the observed data.

Summary of our novel contributions. In this article, we develop a *Robust Chain Graph Model (RCGM)* for multilayered non-Gaussian chain graphs that allows modeling of heavier-than-normal marginal tails in a flexible, data-dependent manner at each layer. Our approach makes multiple contributions:

1. *Methodological contributions:* RCGM provides a highly practical way of bringing non-normality to large graphs by employing Gaussian scale transformations. Node-wise scaling factors are precisely calibrated using empirical marginal tail behaviors. Structural estimation of RCGM uses selection priors on the edges that induce sparsity in the network. RCGM therefore offers the computational advantages of fast high-dimensional graph estimation methods, in addition to accurate adjustments for heavy-tailed marginals in chain graphs.
2. *Theoretical contributions:* RCGM introduces a new Markov property of conditional sign independence that allows for node-specific non-normalities in a chain graph and

interprets dependencies on the original scale of variables (Theorem 2.1). Edges between normal nodes can still be interpreted in terms of conditional independence.

3. *Scientific contributions:* RCGM addresses the growing need in cancer biology research for delineating multiplatform functional drivers of networks underlying drug action. RCGM is designed to handle data needed for such analyses, which come from multiple platforms and often deviate significantly from normality. In our study, RCGM is used to infer the dependency structure within and between CNA, mRNA, RPPA and drug data platforms in lung cancer cell lines. Our analysis encompasses key signaling pathways in human cancers, revealing pathway-level genomic features regulating drug responses. Notable findings include the overall receptivity of the DNA Damage Response (DDR) pathway to drugs, particularly associations of the protein levels of Checkpoint Kinase 1 (CHK1), the main effector of DDR, with drug actions of EGFR TKIs erlotinib and icotinib, which have considerable clinical utility.

The rest of the paper is organized as follows. In Section 2 we introduce the robust chain graph model. Section 3 describes the Bayesian structural estimation procedure. Section 4 provides a comparison of the performance of RCGM with existing GCM alternatives. In Section 5, we analyze the data involving four biological platforms of lung cancer cell lines, to investigate driving mechanisms of drug sensitivities on major lung cancer drugs. Proofs and additional relevant details are presented in the Supplementary Materials. The R codes for the RCGM implementation and data are also available in the supplemental files.

2 Model

Data structure and notations. We consider independent and identically distributed data across cell lines, with $\mathbf{X} = (X_1, \dots, X_q)^T$ denoting data corresponding to a cell line comprising of q coordinates. The q nodes can be partitioned into L disjoint subsets, each subset to be called a layer. Due to existing biological hierarchies, the layers possess an inherent

ordering among themselves and are numbered following that order, such that data in higher layers are regulated by data in lower layers. For instance, in our case study, $L = 4$ and the ordering from layer 1 to 4 is: CNA < mRNA < RPPA < drugs. The dependency structure is modeled by a chain graph, with directed and undirected edges between nodes belonging to different and same layers, respectively. Let $G = (V, E, \mathcal{L})$ denote the chain graph over q nodes, where $V = \{1, \dots, q\}$ is the set of labeled nodes across L layers, E is the set of directed (\rightarrow) and undirected ($-$) edges between nodes in V , and \mathcal{L} is a mapping of node indices to their corresponding layers so that for $v \in V$, $\mathcal{L}(v)$ is the index of the layer in which v is located. For layer l , let $\mathbf{X}_{(l)}$ be the sub-vector of \mathbf{X} with nodes in layer l . Let $\mathbf{X}_{[1:l]}$ denote the sub-vector of nodes in layers 1 to l . Let \mathcal{T}_l be the set of nodes in layer l and $q_l = \sum_{j=1}^l |\mathcal{T}_j|$, where $|A|$ is the number of elements in the set A . Depending on the probability distribution of \mathbf{X} , edges can be characterized in different ways.

2.1 Gaussian Chain Graph Models

A Gaussian chain graph model (GCM) is a multilayered graph where \mathbf{X} follows a multivariate Gaussian distribution. It uses an undirected Gaussian graph to model within layer interactions and a block recursive normal linear simultaneous equations-model to describe dependencies of higher layers on lower layers. This way, the full model is composed of layer-wise normal regression components described by:

$$\mathbf{X}_{(1)} \sim N_{q_1}(\mathbf{0}, \mathcal{J}_1^{-1}), \quad \text{and} \quad \mathbf{X}_{(l)} | \mathbf{X}_{[1:l-1]} \sim N_{|\mathcal{T}_l|}(\boldsymbol{\beta}_l \mathbf{X}_{[1:l-1]}, \mathcal{J}_l^{-1}), \quad l \geq 2, \quad (1)$$

where $\boldsymbol{\beta}_l$ and \mathcal{J}_l are respectively coefficient and precision matrices for the l -th regression component. The model therefore consists of $L - 1$ multiple regressions and one undirected graph in the first layer. Nonzero entries of $\boldsymbol{\beta}_l$ and \mathcal{J}_l respectively encode directed and undirected edges in GCM G . Specifically, $(u - v) \in E$ when the entry corresponding to (u, v) in \mathcal{J}_l equals zero for nodes u and v in the same layer l . Similarly, $(u \rightarrow v) \in E$ when $\boldsymbol{\beta}_l$'s entry for (v, u) is zero, for $\mathcal{L}(u) < \mathcal{L}(v)$ and $\mathcal{L}(v) = l$. By Remark 4.1 and Theorem

4.1 of Andersson et al. (2001), the chain graph G given by (1) follows the alternate Markov property (AMP) where edges are characterized by conditional independence given the AMP conditioning nodes (detailed in Section 2.3), when the true distribution of \mathbf{X} is multivariate normal. Estimation methods for GCM can be found in Drton and Eichler (2006), McCarter and Kim (2014), Lin et al. (2016), Petersen (2018) and Ha et al. (2021), among others.

Although GCMs capture dependencies in multi-level continuous multivariate data, they are inappropriate in settings where marginal distributions are heavy-tailed so that the joint multivariate distribution is no longer Gaussian. An example of a heavy-tailed undirected graph to model such data is the multivariate t -distribution discussed by Finegold and Drton (2011). In chain graphs with heavy-tailed marginals, using a Gaussian model can result in incorrect inferences (Genest and Nešlehová, 2014), and dependencies given by zero structures of β_l and \mathcal{J}_l cannot be interpreted in terms of conditional independence based on the AMP in Andersson et al. (2001). By modeling the marginal non-normal behaviors of nodes, we resolve these issues in a new framework of robust chain graph models that can accurately infer the network and yield interpretable notions of dependencies.

2.2 Robust Chain Graph Models (RCGM)

An effective way to incorporate non-normality arising due to heavy tails is by scale mixture representations with appropriate factors so that the transformed data follow a multivariate Gaussian distribution. Let d_v denote the positive scaling factor for node v such that the $d_v, v \in V$ are independent and have $d_v \sim p_v$ for positive scaling distributions p_v with $\int d_v p_v(d_v) < \infty$. Let \mathbf{D} be a $q \times q$ diagonal matrix with entries $(1/d_1, 1/d_2, \dots, 1/d_q)$, $d_v > 0$. Given d_v 's, the transformed data \mathbf{DX} is assumed to follow a multivariate normal distribution. These random scale transformations have been used in the context of single-layer undirected graphs (Finegold and Drton, 2011, 2014; Bhadra et al., 2018). In our framework of robust chain graphs, we allow flexibility in the marginal behavior through

scale transformations with node-specific degrees of tail-heaviness.

Let \mathbf{D}_l and $\mathbf{D}_{[1:l]}$ denote the sub-matrices of \mathbf{D} corresponding to the nodes $(q_{l-1} + 1)$ to q_l and from 1 to q_l respectively. We define our Robust Chain Graph Model (RCGM) as

$$\begin{aligned} \mathbf{D}_l \mathbf{X}^{(l)} &= \mathbf{B}_l \mathbf{D}_{[1:l-1]} \mathbf{X}_{[1:l-1]} + \boldsymbol{\varepsilon}_l, \quad \boldsymbol{\varepsilon}_l \sim N_{|\mathcal{T}_l|}(\mathbf{0}, \mathcal{K}_l^{-1}), \quad 2 \leq l \leq L, \\ \boldsymbol{\varepsilon}_1 &= \mathbf{D}_1 \mathbf{X}^{(1)}, \quad \boldsymbol{\varepsilon}_1 \sim N_{q_1}(\mathbf{0}, \mathcal{K}_1^{-1}), \end{aligned} \tag{2}$$

where \mathcal{K}_l is the $|\mathcal{T}_l| \times |\mathcal{T}_l|$ precision matrix for the transformed data in the l -th layer and \mathbf{B}_l is a $|\mathcal{T}_l| \times q_{l-1}$ coefficient matrix, and the layer-specific error vectors $\boldsymbol{\varepsilon}_l$ are independent of each other. The independence of $\boldsymbol{\varepsilon}_l$'s ensures that the conditional distribution of $\mathbf{D}\mathbf{X}$ given \mathbf{D} is a multivariate normal distribution given by $\mathbf{D}\mathbf{X}|\mathbf{D} \sim N_q(\mathbf{B}\mathbf{D}\mathbf{X}, \mathcal{K}^{-1})$, where \mathcal{K} is a $q \times q$ precision matrix with entries k_{uv} , \mathbf{B} is a $q \times q$ coefficient matrix, and the sub-matrix of \mathbf{B} corresponding to rows $q_{l-1} + 1$ to q_l and columns 1 to q_{l-1} is equal to \mathbf{B}_l , while that of \mathcal{K} for rows $q_{l-1} + 1$ to q_l and columns $q_{l-1} + 1$ to q_l is \mathcal{K}_l . So given \mathbf{D} , we have $\mathbf{D}\mathbf{X} = \mathbf{B}\mathbf{D}\mathbf{X} + \boldsymbol{\varepsilon}$, $\boldsymbol{\varepsilon} \sim N_q(\mathbf{0}, \mathcal{K}^{-1})$, so that $\mathbf{D}\mathbf{X}|\mathbf{D} \sim N_q(\mathbf{0}, \Omega^{-1})$, $\Omega = (\mathbf{I} - \mathbf{B})^T \mathcal{K} (\mathbf{I} - \mathbf{B})$.

Note that the RCGM in (2) is GCM on the transformed set of variables $\mathbf{D}\mathbf{X}$, and includes GCM as a special case for unit scaling factors for all nodes. When the true distribution is non-normal, dependencies in the E obtained from GCM or RCGM are no longer determined in terms of AMP conditional independence of Andersson et al. (2001). In Section 2.3, we characterize dependencies in the RCGM using a weaker Markov property.

2.3 Characterization of Dependencies in RCGM

The edge set E may hold different statistical interpretations of dependencies, depending on the true probability distribution of the chain graph. The RCGM as described in (2) is constructed in a way to satisfy AMP of Andersson et al. (2001) in a Gaussian population. The AMP specifies a direct mode of data generation and provides an easily interpretable statistical characterization of directed and undirected edges in chain graph models. In non-normal populations, however, RCGM does not satisfy the AMP, as nonzero entries

of $(\mathbf{B}, \mathcal{K})$ may not imply conditional independence. Nevertheless, edges in RCGM can be characterized in terms of the dependencies defined as follows:

Definition 2.1 *We define four types of relations between random variables Y_1 and Y_2 with a conditioning random vector \mathbf{Z} .*

(i) Y_1 and Y_2 are said to be conditionally sign-independent (CSI) given \mathbf{Z} , denoted by $Y_1 \perp\!\!\!\perp^s Y_2 | \mathbf{Z}$, if $P(Y_1 < 0 | \mathbf{Z}) = P(Y_1 < 0 | Y_2, \mathbf{Z})$ and $P(Y_2 < 0 | \mathbf{Z}) = P(Y_2 < 0 | Y_1, \mathbf{Z})$, whenever the conditional probabilities exist. Otherwise, Y_1 and Y_2 are conditionally sign-dependent (CSD) given \mathbf{Z} .

(ii) Y_1 and Y_2 are said to be conditionally independent (CI) given \mathbf{Z} , denoted by $Y_1 \perp\!\!\!\perp Y_2 | \mathbf{Z}$, if $f(Y_1 | \mathbf{Z}) = f(Y_1 | Y_2, \mathbf{Z})$ and $f(Y_2 | \mathbf{Z}) = f(Y_2 | Y_1, \mathbf{Z})$, where f denotes the corresponding probability density functions, whenever the conditional probability densities exist. Otherwise, Y_1 and Y_2 are conditionally dependent (CD) given \mathbf{Z} .

As a simple illustration, consider $Y_1 \sim N(0, 1)$, $Y_2 = UY_1$, $Z \sim N(0, 1)$, where $U \sim \text{Unif}(-1, 1)$, and U and Z are independent of Y_1 . Then (Y_1, Y_2) are conditionally sign-independent given Z . The concept of CSI in Definition 2.1 (i) is defined in terms of the sign rather than the magnitude, which was introduced in Bhadra et al. (2018) for undirected networks, implying that sign of Y_1 is independent from that of Y_2 , conditioned on \mathbf{Z} . Thus, CSI is weaker than CI. However, the advantage is that it applies to less restrictive multivariate models where the normality assumption can be relaxed.

In our RCGM model (2) that allows both normal and non-normal nodes, we aim to characterize the edges in terms of CSI and CI on the original random variables \mathbf{X} . We model the node-specific non-normality behavior by introducing indicators ω_v that takes the value 1 if X_v has tails heavier than normal ($d_v \sim p_v$) and 0 if X_v is normal ($d_v = 1$). Edge interpretations can be obtained from Theorem 2.1.

Theorem 2.1 (i) *(At least one node is non-normal). If $\omega_u = 1$ or $\omega_v = 1$, conditional sign-independence follows from \mathbf{B} and \mathcal{K} as:*

- (a) (*u and v in the same layer*). Suppose $\mathcal{L}(u) = \mathcal{L}(v)$ and $\rho = k_{uv} = k_{vu}$. Then $\rho = 0$ if and only if $X_u \perp\!\!\!\perp^s X_v | \mathbf{Z}_u$, where $\mathbf{Z}_u = \mathbf{X}_{[1:\mathcal{L}(u)]} \setminus \{X_u, X_v\}$.
- (b) (*u and v in different layers*). Suppose $\mathcal{L}(u) < \mathcal{L}(v)$ and $\rho = \mathbf{B}_{vu}$. Then $\rho = 0$ if and only if $X_u \perp\!\!\!\perp^s X_v | \mathbf{Z}_d$, where $\mathbf{Z}_d = \mathbf{X}_{[1:\mathcal{L}(v)-1]} \setminus X_u$.
- (ii) (*Between normal nodes*). Suppose $\omega_u = \omega_v = 0$, and ρ is as defined in part (i). Then $\rho = 0$ if and only if $X_u \perp\!\!\!\perp X_v | \mathbf{Z}_u$ for $\mathcal{L}(u) = \mathcal{L}(v)$ and $X_u \perp\!\!\!\perp X_v | \mathbf{Z}_d$ for $\mathcal{L}(u) < \mathcal{L}(v)$.

The proof is in Supplementary Section S.1.1 - S.1.2. Note that the conclusion (ii) of Theorem 2.1 is the same as the AMP of Andersson et al. (2001). Theorem 2.1 shows that the interpretation of E given by RCGM depends on the node-specific marginal distributions of the corresponding random variables. The types of dependencies and the way they are related to each other are demonstrated in Figure 2 and summarized as follows:

- *CSI and CI*. A missing edge between two nodes is interpreted as conditional sign-independence (CSI) when at least one of the nodes is non-normal by part (i) of Theorem 2.1. When both nodes follow normal distributions, by part (ii) of the theorem, the absence of an edge between two nodes is interpreted as conditional independence (CI) which is a stronger form of the Markov property.
- *CSD and CD*. The non-zero entries of \mathbf{B} and \mathcal{K} are interpreted as conditional sign-dependence (CSD) which implies conditional dependence (CD) when at least one of the corresponding nodes is non-normal. Thus, edges connecting non-normal nodes are considered to have stronger relation than edges between normal nodes.

Another notion of dependency, the partial correlation, is defined as the correlation between variables after adjusting for the effects of conditioning variables, and the zero values are equivalent to conditional independence in a Gaussian population. However, as the zero structure is preserved under random and independent marginal scale transformations (see Section 5.1 of Finegold and Drton (2011)), partial correlation interpretations of edges do not hold in non-Gaussian populations, as explained in Remark 2.1.

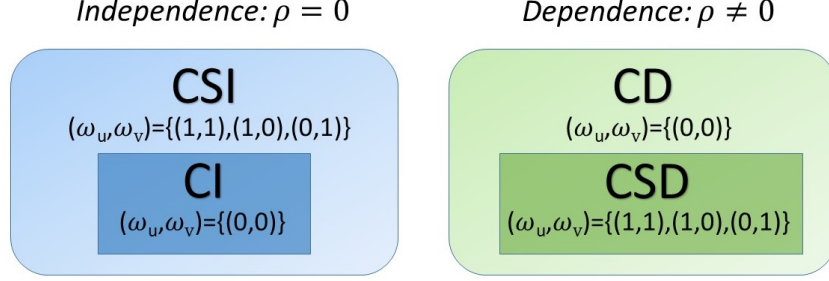


Figure 2: The nested relation between CSI, CI, CD and CSD (Definition 2.1). For $\mathcal{L}(u) = \mathcal{L}(v)$, $\rho = \mathcal{K}_{uv}$. For $\mathcal{L}(u) < \mathcal{L}(v)$, $\rho = \mathbf{B}_{vu}$. ω_v is the indicator of v being non-normal. For missing edges ($\rho = 0$) in G , CI is the stronger form of independence as compared to CSI while for edges ($\rho \neq 0$) in G , CSD is stronger than CD in terms of dependence.

Remark 2.1 *Neither of the edge sets E obtained under GCM or RCGM can be interpreted in terms of partial correlations between original variables under non-normal data, as evaluating partial correlations involves the true probability distribution. RCGM yields CSI interpretations of E , which is the main advantage of using RCGM over GCM in the non-normal network estimation scenario.*

2.4 Incorporating a Continuous Measure of Non-normality

To allow for more flexibility in the proposed framework, we incorporate a mixture model for the amount of non-normality by introducing a variable π_v for node v which quantifies the departure of the node’s distribution from that of a normal distribution. We treat the non-normality status ω_v of each node as random, and model $P(\omega_v = 1) = \pi_v$, a priori, so that the larger π_v indicates a higher degree of prior belief regarding departure from normality for node v . We formulate our final model as

$$\mathbf{DX} | \mathbf{D}, \boldsymbol{\omega}, \boldsymbol{\pi} \sim N(\mathbf{BDX}, \mathcal{K}^{-1}), \quad d_v | \boldsymbol{\omega}, \boldsymbol{\pi} \sim \omega_v p_v + (1 - \omega_v) \delta_1, \quad \omega_v | \pi_v \sim \text{Bern}(\pi_v), \quad (3)$$

where $\pi_v \in [0, 1]$ for all $v \in V$ and $\boldsymbol{\pi} = (\pi_1, \dots, \pi_q)$. By considering ω_v as random under model (3), the strength of dependencies are interpreted in a continuous scale calibrated by probabilities rather than deterministically as in Theorem 2.1.

Model selection-based network inference methods commonly assign a probability score g_{uv} to each edge, which indicates its probability of being present in the network. The

edge-wise probability score g_{uv} and node-wise non-normality scores (π_u, π_v) are combined to characterize the dependence properties for a network, by the following corollary to Theorem 2.1, with a proof in Supplementary Section S.1.3.

Corollary 2.2 *Let g_{vu} be the probability of edge $(u - v)$ or $(u \rightarrow v)$ being present in the model under $\mathcal{L}(u) = \mathcal{L}(v)$ and $\mathcal{L}(u) < \mathcal{L}(v)$ respectively. Then $X_u \perp\!\!\!\perp^s X_v | \mathbf{Z}$ with probability $(1 - g_{vu})$ and $X_u \perp\!\!\!\perp X_v | \mathbf{Z}_u$ with probability at least $(1 - g_{vu})(1 - \pi_u - \pi_v + \pi_u \pi_v)$ for $\mathbf{Z} = \mathbf{X}_{[1:\mathcal{L}(u)]} \setminus \{X_u, X_v\}$ when $\mathcal{L}(u) = \mathcal{L}(v)$ and $\mathbf{Z} = \mathbf{X}_{[1:(\mathcal{L}(v)-1)]} \setminus X_u$ when $\mathcal{L}(u) < \mathcal{L}(v)$.*

Corollary 2.2 provides a probabilistic characterization of edges in RCGM on the original scale of nodes, from CSI to CI for missing edges, and equivalently CD to CSD for edges, depending on the probabilities of edge inclusion and node non-normality. In summary, the multilayered network inference using RCGM in (3) allows a robust structural recovery of chain graphs when the marginals deviate from normal distributions, along with calibration of node-specific marginal tail-heaviness through π_v , and dependence characterization of the network structures on the original variables weighted by the strength from CSD to CD.

3 Bayesian Estimation of RCGM

Estimation of the multilayered network incorporating uncertainty in node-wise normality involves two parameters \mathbf{B} and \mathcal{K} for the graphical structure and $\boldsymbol{\pi}$ for the degree of non-normality in model (3). We use a Bayesian framework with a Markov chain Monte Carlo (MCMC) sampling scheme to draw posterior samples of the parameters. Since the RCGM is formulated in layer-wise multivariate regressions (Equation (2)), we perform each regression by imposing priors independently across layers. At each MCMC iteration, for each layer l , we update the structural parameters \mathbf{B}_l and \mathcal{K}_l , following a scale transformation of the data using sampled scaling factors with $\boldsymbol{\pi}_l$. For Sections 3.1 – 3.3, let \mathbf{x}_v and \mathbf{d}_v respectively denote the $n \times 1$ vectors of data \mathbf{X} and scaling matrix \mathbf{D} corresponding to node v .

3.1 Prior Calibration for Node-wise Non-normality

The prior specifications of node non-normality are conducted based on empirical marginal distributions. We assume that π_v follows a beta distribution

$$\pi_v \sim \text{Beta}(\mu_v r_v, (1 - \mu_v) r_v),$$

where μ_v is the prior mean and r_v is to control the variance. The mean and variance are decided based on the degree of non-normality evaluated from data for each node. Specifically, we set μ_v by the H score defined as $H(\mathbf{x}_v) = 2 * \Phi(\log(1 - pval(\mathbf{x}_v)))$ from the p -value of the test for normality of the marginal distribution of X_v from the Kolmogorov-Smirnov test. We choose r_v to ensure a small variance (e.g., 0.01) for the prior distribution to be concentrated around $H(\mathbf{x}_v)$ on the unit interval.

The mixing distribution p_v in the model (3) is determined by empirically evaluating the tail behavior of marginals for each node. The marginal tail mass appearing as exponential or polynomial decay is related to exponential or polynomial tail behavior of p_v respectively (Bhadra et al., 2018). We assume that every heavy-tailed marginal centered at its median is a univariate- t or a double exponential distribution with non-centrality or a location parameter of zero respectively, so that there are two categories of p_v - polynomially decaying such as an Inverse-Gamma, and exponentially decaying as in the Gamma and Exponential distributions. We regress $\log \hat{f}(\mathbf{x}_v)$, the log-transformed smoothed empirical probability density estimate of the marginal distribution, on $\log \mathbf{x}_v$ and \mathbf{x}_v . We then determine for which category (polynomial/exponential) the regression p -value is smaller and estimate the coefficients for $\log \mathbf{x}_v$ and \mathbf{x}_v in this category. The estimated coefficients are then used to derive the parameters of the chosen p_v using Algorithm 2 in Supplementary Section S.4.

3.2 Priors on Model Selection Parameters

The scaling factors d_v are generated using the non-normality parameters π_v from Section 3.1. As RCGM becomes a GCM for the scaled variables when d_v are given (Equation (2)), \mathbf{B} and \mathcal{K} can be estimated based on the scaled data by building Gaussian and Wishart

priors for the layer-wise regression parameters \mathbf{B}_l and \mathcal{K}_l . However, in chain graphs with multiple large layers, the set of parameters becomes extensive with the number and size of layers, in addition to becoming increasingly sparse (Armstrong, 2005). Significant computational challenges appear even in moderately large graphs. Instead, we simultaneously select undirected and directed edges connected to a node v belonging to layer l , using a stochastic search variable selection framework (SSVS) (George and McCulloch, 1993) after coherently reparameterizing the precision parameter \mathcal{K}_l into regression coefficients to yield the node-conditional likelihoods (Ha et al., 2021). For v , the node-wise regression is

$$\frac{X_v}{d_v} = (\mathbf{X}\mathbf{D})_{[1:l-1]}^T (\mathbf{b}_v - \mathbf{B}_l^{(v)} \mathbf{a}_v) + (\mathbf{X}\mathbf{D})_{\mathcal{T}_l \setminus v}^T \mathbf{a}_v + e_v, \quad (4)$$

where $\mathbf{a}_v = -k_{vv} \mathbf{k}_l^{(v)}$, where $\mathbf{k}_l^{(v)}$ is the vector of k_{vu} , $u \in \mathcal{T}_l \setminus v$, and $e_v \sim N(0, k_{vv}^{-1})$. The parameters of interest in each node-conditional likelihood are \mathbf{b}_v , \mathbf{a}_v , $\mathbf{B}_l^{(v)}$, and k_{vv} , where the effect of nodes in layers $1 : (l-1)$ on v is depicted by \mathbf{b}_v , while their effect on nodes in $\mathcal{T}_l \setminus v$ is denoted by $\mathbf{B}_l^{(v)}$, and \mathbf{a}_v is the effect of the neighbors of node v in \mathcal{T}_l on v . Details can be found in Supplementary Section S.2. However, as \mathbf{b}_v , \mathbf{a}_v , and $\mathbf{B}_l^{(v)}$ are not jointly identifiable (Supplementary Section S.3), we fix $\mathbf{B}_l^{(v)}$ at its current value in each MCMC iteration and consider the node-conditional likelihood with parameters \mathbf{b}_v , \mathbf{a}_v and k_{vv} .

We set priors on the parameters of each node-wise regression for estimating \mathbf{B}_l and \mathcal{K}_l in the model (3). As shown in the equation (10) of Ha et al. (2021), Wishart and independent Gaussian priors on \mathbf{B}_l and \mathcal{K}_l respectively are equivalent to independent Gaussian and Gamma priors on $\{\mathbf{b}_v, \mathbf{a}_v\}$ and k_{vv} . We let γ_{vw} and η_{vu} be the indicator variables encoding zero-structures of \mathbf{B} and \mathcal{K} , with $P(\gamma_{vu} = 1) = p_{vw}$, and $P(\eta_{vu} = 1) = q_{vu}$ for $p_{vw}, q_{vu} \in (0, 1)$. We use a spike-and-slab prior similar to Ha et al. (2021) to set priors as

$$\begin{aligned} b_{vw} | \gamma_{vw}, k_{vv} &\sim \gamma_{vw} N(0, c_{vw}^2 / k_{vv}) + (1 - \gamma_{vw}) \delta_0, \\ a_{vu} | \eta_{vu}, k_{vv} &\sim \eta_{vu} N(0, 1 / (\lambda_l k_{vv})) + (1 - \eta_{vu}) \delta_0, \\ k_{vv} &\sim \text{Gamma}((\delta_l + |\mathcal{T}_l| - 1) / 2, \lambda_l / 2), \end{aligned}$$

Algorithm 1: MCMC sampling steps for iteration t .

At iteration t , update \mathbf{D} given current $\boldsymbol{\pi}$ for every subject by Metropolis-Hastings sampling using Equation (S.11).

for $1 \leq l \leq q_L$ **do**

for $v \in \mathcal{T}_l$ **do**

 Update π_v using Metropolis Hastings sampling (Equation (S.12))

 Update the undirected edges:

1. Set response $\tilde{\mathbf{x}}_v = \mathbf{x}_v/\mathbf{d}_v - \mathbf{X}_{[1:l-1]}^T \mathbf{D}_{[1:l-1]} \mathbf{b}_v$ and covariates \mathbf{Z}_v as $\mathbf{D}_{\mathcal{T}_l \setminus v} \mathbf{X}_{\mathcal{T}_l \setminus v} - \mathbf{B}_{\mathcal{T}_l \setminus v, [1:l-1]} \mathbf{D}_{[1:l-1]} \mathbf{X}_{[1:l-1]} = \boldsymbol{\epsilon}_{\mathcal{T}_l \setminus v}$.
2. Update $\{\boldsymbol{\eta}_w : w \in \mathcal{T}_l\}$ by an add/delete/swap step and MH-selection thereafter. Set the neighborhood of v as $\text{ne}_v^u = \{w \in \mathcal{T}_l : \eta_{vw} \neq 0\}$. Set $\eta_{vw} = \eta_{vw}$ for every $w \in \text{ne}_v^u$.
3. Update the coordinates of \mathbf{a}_v that were selected into ne_v^u and k_{kk} using Gibbs sampling through Equations (S.13) and (S.14).

 Update the directed edges:

1. Set $\tilde{\mathbf{x}}_v = \mathbf{x}_v/\mathbf{d}_v - \boldsymbol{\epsilon}_{\mathcal{T}_l \setminus v}^T \mathbf{a}_v$, $\mathbf{Z}_v = \mathbf{D}_{[1:l-1]} \mathbf{X}_{[1:l-1]}$, where $\boldsymbol{\epsilon}_{\mathcal{T}_l \setminus v}$ is equal to $\mathbf{D}_{\mathcal{T}_l \setminus v} \mathbf{X}_{\mathcal{T}_l \setminus v} - \mathbf{B}_{\mathcal{T}_l \setminus v, [1:l-1]} \mathbf{D}_{[1:l-1]} \mathbf{X}_{[1:l-1]}$.
2. Update $\{\boldsymbol{\gamma}_w : w \in \mathcal{P}_l\}$ using add/delete/swap and MH-selection. Set $\text{ne}_v^d = \{w \in \mathcal{P}_l : \gamma_{vw} \neq 0\}$, where \mathcal{P}_l is the set of nodes in layers 1 to $l-1$.
3. Update the coordinates of \mathbf{b}_v that were selected into ne_v^d and k_{vv} using Gibbs sampling through Equations (S.15) and (S.16).

end

end

for $c_{vw}, \lambda_l, \delta_l > 0$ and δ_0 denotes the degenerate distribution at 0. The MCMC algorithm is run layer-wise at each iteration, wherein the scaled node-wise likelihoods corresponding to nodes in \mathcal{T}_l (in random order of nodes) are combined with the priors to yield posterior samples for \mathbf{b}_v , \mathbf{a}_v and k_{vv} keeping $\mathbf{B}_l^{(v)}$ fixed.

3.3 Posterior Sampling

Posterior samples of \mathbf{B} , \mathcal{K} and $\boldsymbol{\pi}$ are constructed from the parameters \mathbf{b}_v , \mathbf{a}_v , k_{vv} and π_v in node-wise regressions (Equation (S.9)), which are drawn using the MCMC sampling scheme

summarized in Algorithm 1, with detailed derivations in Supplementary Section S.5. A maximum a posteriori (MAP) estimate across the MCMC samples may be hard to derive in huge model spaces, and provides no probabilistic quantification of uncertainty in the parameters. Instead, we use the marginal posterior edge inclusion probability g_{uv} , which is the proportion of times in MCMC runs after burn-in that the edge ($u - v$ or $u \rightarrow v$) is included. Fixing the false discovery rate (FDR) α in $(0, 1)$, we determine a cutoff C_α by sorting all g_{uv} in decreasing order to obtain $g_{(t)}$, and setting $C_\alpha = g_{(\xi)}$, where $\xi = \max\{k : k^{-1} \sum_{t=1}^k (1 - g_{(t)}) < \alpha\}$. We then form the set of edge discoveries $\chi_\alpha = \{(u, v) : g_{uv} > C_\alpha\}$. We similarly evaluate the sign of an edge by the sign of coordinate-wise average of \mathbf{B} or \mathcal{K} , and the non-normality probabilities π_v , using the corresponding averages across MCMC samples. We combine posteriors for the node non-normalities (π_u, π_v) and the edge inclusion probability g_{uv} to assign weight for an edge between nodes u and v that represents the strength of dependence from CSD to CD based on Corollary 2.2.

4 Simulations

We conduct simulation experiments to evaluate the performance of our RCGM framework, in terms of graph structure recovery, as compared to other GCM-based methods, under various non-normality mechanisms. We generate simulation datasets based on the model in Equation (3) corresponding to random chain graphs with q nodes that are divided into L ordered layers with similar sizes. The layer-wise undirected graphs are formed by randomly connecting two nodes with probability p_E independent of all other edges. We then connect two nodes in different layers independently with probability $p_E/2$, where the directions follow the order among the L layers. Thus directed edges between layers are less likely to be connected than the undirected edges within a layer. Given the chain graph, we set the corresponding nonzero elements of \mathbf{B} and \mathcal{K} by random samples from a uniform distribution in $(-1.5, -0.5) \cup (0.5, 1.5)$ and ensure positive definiteness of \mathcal{K}

by imposing diagonal dominance. We consider pre-fixed non-normality score $\pi \in [0, 1]$ and scale-mixing distribution p_v for coordinate v for each simulation dataset. For every π and p_v combination, we impose node-wise heavy tails on each sample by generating $\omega_v \sim \text{Bernoulli}(\pi)$, $d_v \sim p_v$ if $\omega_v = 1$, $d_v = 1$ otherwise and then transforming the sample as $(X_1, \dots, X_q) \mapsto (X_1 d_1, \dots, X_q d_q)$. We repeat this process for all the n samples generated from the Gaussian chain graph model. We consider mixing distributions with two types of tails - exponential with p_v as the exponential distribution with mean 2.5, and polynomial where p_v is Inverse-Gamma with shape 3 and scale 6. We vary π across a range of values in $(0, 1)$ corresponding to low ($\pi = 0.05$), medium ($\pi = 0.60$) and high ($\pi = 0.95$) levels of non-normality, expecting RCGM to perform better than GCMs for datasets with higher π .

We compare RCGM’s performance with that of the Bayesian node-wise Gaussian approach (Ha et al., 2021) and the penalized Gaussian likelihood approach (Lin et al., 2016), using BANS and LBBM respectively to refer to these methods. We use 4,000 burn-in samples and 10,000 samples for posterior inference in both RCGM and BANS, and determine the cutoffs on edge inclusion posterior probabilities in both methods by controlling the FDR at 0.1. As suggested by Lin et al. (2016), we use glasso (Friedman et al., 2008) to estimate the undirected graph in the first layer by LBBM. Table 1 displays the performance of the three methods across three values of π in terms of the metrics described as *Specificity* = $TN/(TN + FP)$, *Sensitivity* = $TP/(TP + FN)$, and Matthew’s correlation coefficient $MCC = [(TP \times TN) - (FP \times FN)] / \{[(TP + FP)(TP + FN)(TN + FP)(TN + FN)]^{1/2}\}$ that ranges from -1 (complete non-concordance) to 1 (full concordance). Across various tuning parameters for LBBM and cutoffs for the posterior probability of edge inclusion for BANS and RCGM, the performance is evaluated based on area under the ROC curve (AUC). We calculate the partial area under ROC curve (pAUC) by evaluating the area under the curve between specificity ranging from 0.8 or 0.9 to 1 and dividing it by the maximum possible AUC in that range.

$(q, L, p_E) = (50, 4, 0.08), p_v : \text{Exponential}(\text{mean} = 2.5)$							
Setting	Method	Specificity	Sensitivity	MCC	AUC	pAUC 0.9	pAUC 0.8
$(\pi = 0.95)$	RCGM	0.965 (0.006)	0.812 (0.068)	0.759 (0.046)	0.902 (0.036)	0.755 (0.013)	0.795 (0.016)
	BANS	0.922 (0.005)	0.768 (0.088)	0.701 (0.062)	0.868 (0.042)	0.684 (0.011)	0.788 (0.016)
	LBBM	0.905 (0.005)	0.672 (0.088)	0.655 (0.064)	0.874 (0.041)	0.731 (0.013)	0.760 (0.016)
$(\pi = 0.60)$	RCGM	0.948 (0.007)	0.838 (0.064)	0.787 (0.052)	0.916 (0.038)	0.752 (0.035)	0.791 (0.091)
	BANS	0.939 (0.007)	0.783 (0.077)	0.738 (0.063)	0.851 (0.044)	0.735 (0.017)	0.780 (0.022)
	LBBM	0.940 (0.005)	0.780 (0.088)	0.731 (0.064)	0.858 (0.039)	0.738 (0.013)	0.780 (0.016)
$(\pi = 0.05)$	RCGM	0.945 (0.007)	0.850 (0.061)	0.821 (0.055)	0.962 (0.021)	0.828 (0.017)	0.874 (0.022)
	BANS	0.955 (0.009)	0.848 (0.072)	0.820 (0.063)	0.945 (0.027)	0.820 (0.035)	0.871 (0.091)
	LBBM	0.912 (0.005)	0.802 (0.088)	0.792 (0.061)	0.919 (0.042)	0.795 (0.013)	0.851 (0.016)

$(q, L, p_E) = (50, 4, 0.08), p_v : \text{Inverse-Gamma}(\text{shape} = 3, \text{scale} = 6)$							
Setting	Method	Specificity	Sensitivity	MCC	AUC	pAUC 0.9	pAUC 0.8
$(\pi = 0.95)$	RCGM	0.995 (0.007)	0.657 (0.064)	0.604 (0.052)	0.873 (0.044)	0.706 (0.035)	0.748 (0.091)
	BANS	0.996 (0.007)	0.528 (0.077)	0.553 (0.063)	0.833 (0.046)	0.698 (0.017)	0.734 (0.022)
	LBBM	0.882 (0.019)	0.657 (0.041)	0.557 (0.059)	0.845 (0.052)	0.683 (0.043)	0.745 (0.036)
$(\pi = 0.60)$	RCGM	0.996 (0.006)	0.642 (0.078)	0.610 (0.056)	0.902 (0.029)	0.770 (0.032)	0.781 (0.089)
	BANS	0.996 (0.009)	0.557 (0.075)	0.527 (0.068)	0.812 (0.052)	0.726 (0.018)	0.754 (0.025)
	LBBM	0.879 (0.036)	0.657 (0.052)	0.535 (0.071)	0.831 (0.051)	0.723 (0.074)	0.770 (0.076)
$(\pi = 0.05)$	RCGM	0.990 (0.006)	0.757 (0.081)	0.604 (0.051)	0.961 (0.025)	0.805 (0.020)	0.840 (0.018)
	BANS	0.994 (0.007)	0.748 (0.091)	0.598 (0.062)	0.952 (0.027)	0.803 (0.017)	0.832 (0.019)
	LBBM	0.877 (0.032)	0.771 (0.044)	0.583 (0.036)	0.901 (0.034)	0.773 (0.059)	0.804 (0.061)

Table 1: Performance of RCGM as compared to BANS and LBBM under Exponential and Inverse-Gamma scaling distributions p_v , and low, medium and high levels of non-normality indexed by $\pi = 0.05, 0.60, 0.95$ respectively, and $(q, L, n, p_E) = (50, 4, 200, 0.08)$ where q, L, n and p_E denote the dimension of the graph, number of layers, sample size and sparsity respectively. pAUC 0.9 is the (scaled) area under the ROC curve when specificity is fixed at 0.9 (1-specificity is fixed at 0.1). Results are summarized across 30 replications; standard errors are within parentheses. The winning entry for each metric is displayed in bold.

We observe that performance of all the methods deteriorates gradually as more non-normality is induced through increasing π . While the three methods almost coincide for near-normal data when $\pi = 0.05$, RCGM performs significantly better than the Gaussian methods for data with medium and high degree of non-normality (Table 1). Therefore RCGM performs as good as GCMs in normal data, and consistently better than GCMs as tails become heavier than normal. Analysis of ROC curves reveals a relatively weaker performance of all the methods for medium non-normality ($\pi = 0.60$) as compared to high non-normality ($\pi = 0.95$), and a bigger contrast between RCGM and GCM methods in medium π as compared to that in high π (Figure 3). Simulations over an extended set of π values with $\pi = \{0.01, 0.05, 0.4, 0.6, 0.8, 0.9, 0.95, 0.99\}$ show a similar pattern (Figure S.2),

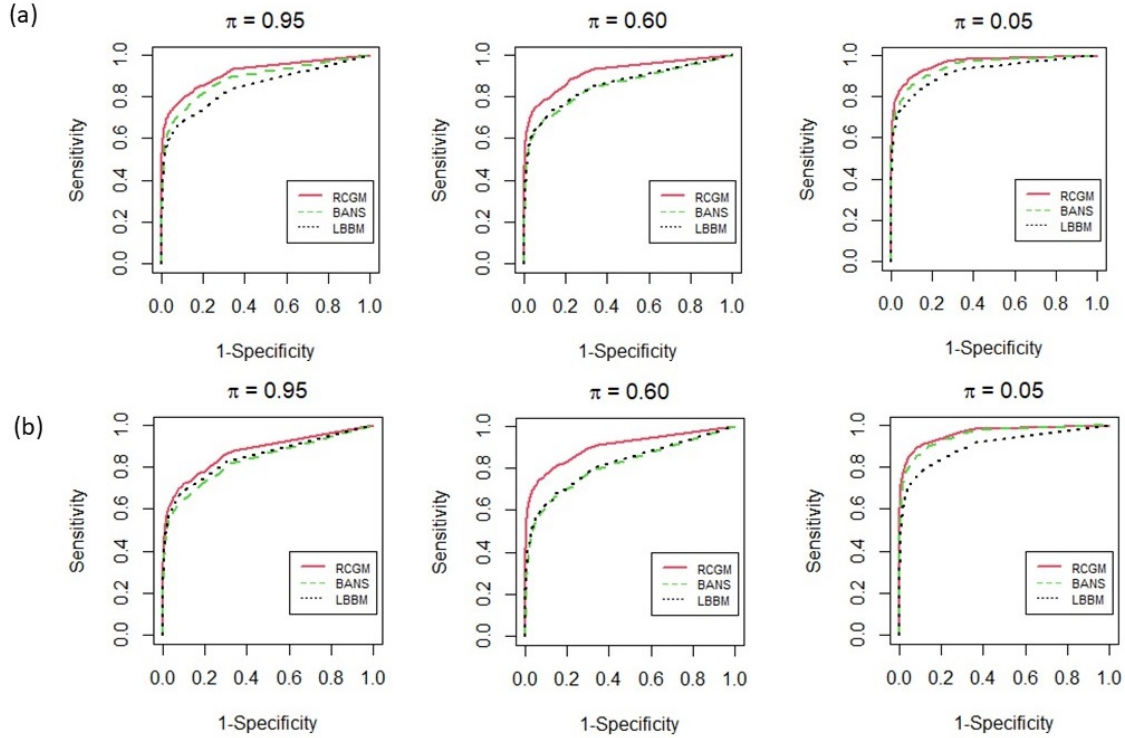


Figure 3: ROC curves for the simulation setting $(q, L, n, p_E) = (50, 4, 200, 0.08)$ across high, medium and low levels of non-normality π , where q , L and p_E denote the dimension of graph, number of layers and sparsity respectively. Panels (a) and (b) correspond to scaling by Exponential(mean = 2.5) and Inv-Gamma(shape = 3, rate = 6) respectively.

where the AUCs are lower for $\pi = 0.4$ to $\pi = 0.8$ than for $\pi \geq 0.9$, and the maximum contrast between RCGM and GCM AUCs is found in the medium non-normality range $\pi \in [0.4, 0.8]$. The possible reason behind this could be the higher level of tail-heaviness in the data induced by π in the range $\pi = 0.2$ to $\pi = 0.8$. Our algorithm is designed to tackle data with heavy-tailed marginals, so the difference between performances of RCGM and Gaussian methods becomes more prominent with increased tail-heaviness, which occurs in the range $\pi = 0.2$ to $\pi = 0.8$. Further details can be found in Supplementary Section S.6.

5 Pharmacogenomics in Lung Cancer

Integrative data analysis and the use of network topology towards functional characterization of drug sensitivity is critical to the successful development of cancer treatments

(Kasarskis et al., 2011). Our aim is to understand mechanisms of drug action by modeling the complex regulatory and interactive processes across various domains of the molecular data. A public resource for high-throughput screening data on more than 4,000 drugs for 578 cell lines spanning 24 human tumor types was created by Corsello et al. (2020) from the CCLE project (Barretina et al., 2012). Growth inhibitory activity defined as drug sensitivity was measured in terms of log-transformed median fluorescence intensity (MFI) of barcoded cell lines after drugs were administered. Lower log-MFI values correspond to lower cell viability and therefore higher drug sensitivity. We use these drug screening data along with copy number aberration (CNA), mRNA expression (mRNA), and RPPA-based protein expression (RPPA) (Ghandi et al., 2019) obtained from the DepMap Portal (www.depmap.org). We select $n = 104$ lung cancer cell lines and match them across the CNA, mRNA, RPPA and drug platforms. Sixteen drugs that have been evaluated in clinical trials for different types of lung cancer, are found in the PRISM database and are selected for the study. Based on the mechanism of action, these drugs can be categorized into EGFR-TKIs, ALK-TKIs, tubulin polymerization inhibitors among several other categories (Tables S.3 – S.4). Four of these drugs - Cisplatin, Sevoflurane, Carboplatin and Sorafenib - that have been studied for potential combination therapies for NSCLC (Liang et al., 2013; Langer et al., 1995; Gridelli et al., 2011), are also selected to explore their functional mechanisms. Features in each platform constitute a layer, and the order CNA<mRNA<RPPA<drugs is justified by the biological process that CNA affects mRNA gene expressions, which are then translated into protein, and genes and proteins regulate drug response as a phenotype (Morris and Baladandayuthapani, 2017).

We perform pathway-wise analyses that define multi-platform functional cancer networks for each pathway, based on literature outlining abnormalities of cell signaling pathways as etiology of cancers including lung (Vogelstein and Kinzler, 2004; Brambilla and Gazdar, 2009). We select genes/proteins that are involved in the 10 most clinically tar-

getable signaling pathways in human cancers, as defined in Akbani et al. (2014). The gene and antibody of RPPA membership for each pathway is provided in Table S.2. We apply RCGM on each pathway-level multilayered data, using a burn-in sample size of 2,000 and 10,000 samples for posterior inference of edge-inclusion probabilities g_{vu} and non-normality scores π_v . Controlling FDR at 0.1, we selected edges that have posterior probabilities of edge inclusion greater than 0.55 across all pathways.

The size of the parameter space in each pathway-level network is fairly large - the average number of nodes and number of parameters for edge inclusion and non-normality probabilities has an average of 46.2 and 1090.32 across pathways respectively. The computation time is reasonable, as the average time taken for estimating each network is 4.32 hours with a standard deviation of 0.86 across pathways, on a 3.5 GHz Intel Core i7 processor.

In our robust multilayered networks, the edges are weighted and colored by the dependence characterization of the RCGM discussed in Sections 2.3-2.4. Two nodes u and v are connected and weighted by probability g_{vu} , to represent the strength from CD to CSD based on Corollary 2.2. With node labels for non-normal marginals if $\hat{\pi}_v > 0.5$, we further categorize the edges as CD if both are normal and CSD otherwise. An inter-platform connectivity analysis across pathways is displayed in Figure 4, and the pathway-level multilayered networks are displayed in Figure 5 and Figures S.6 – S.14. We further evaluate the extent of non-normality in the data and find high variability in within-platform non-normal behavior (Figure S.4), similar to the H -scores for empirical non-normalities (Figure 1d). The posterior non-normality probabilities $\hat{\pi}_v$ are positively correlated with H -scores (Figure S.15).

5.1 Inter-platform Regulatory Network

Based on the estimated networks across all 10 pathways, we investigate inter-platform regulatory signaling patterns at the pathway-level in the Sankey diagram (Figure 4). It demonstrates the connectivity between platforms within each pathway, and the drugs.

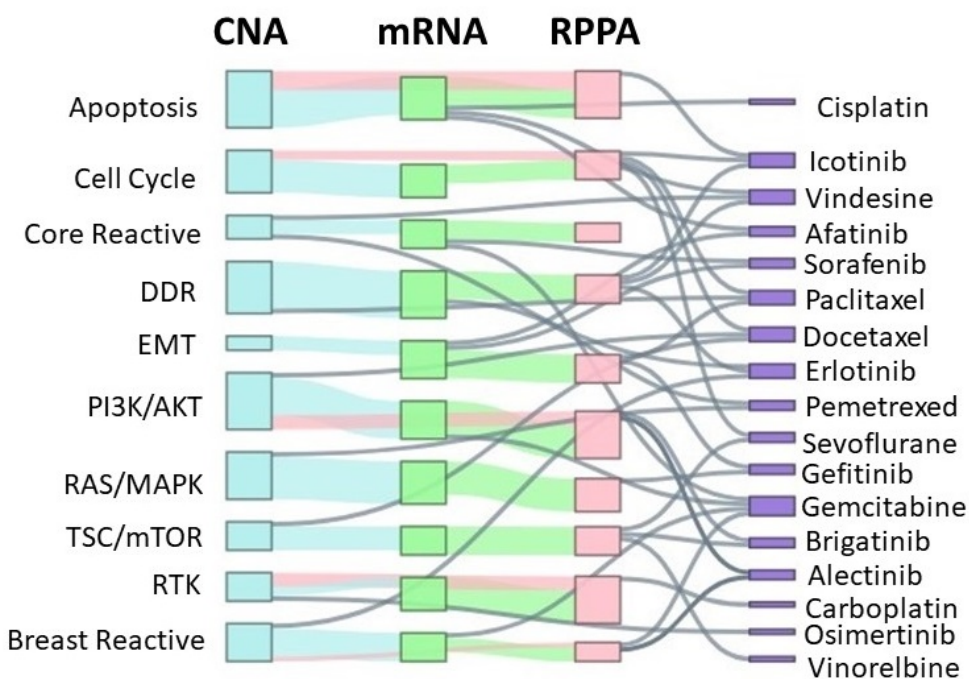


Figure 4: Sankey diagram showing connectivity between the 4 platforms across 10 pathways. Each box in the left three columns is a pathway-molecular platform combination, and widths of the lines between them are proportional to the number of directed edges connecting them. Gray lines denote edges between pathway-platform blocks and drugs.

Each unit is a pathway-platform combination depicted by a box and the lines between units are proportional to the number of directed edges between platforms within pathways. Sizes of the unit boxes are proportional to the degree, and larger boxes, therefore, represent higher levels of regulatory signaling coming in and out the pathways and drugs. The total number of directed edges between molecular platforms are 61 for CNA→mRNA, 56 for mRNA→RPPA and 13 for CNA→RPPA, indicating that as expected, the immediate platforms are tightly connected across pathways. Apoptosis and PI3K/AKT pathways have the most cross-platform signaling, with 8, 6, and 4 edges for CNA→mRNA, mRNA→RPPA and CNA→RPPA respectively in Apoptosis, and 8, 7, and 3 edges respectively in PI3K/AKT. We investigate the regulatory factors to the drugs- CNA, mRNA and RPPA have 8, 10, and 17 edges connected to any of the drugs, which implies that proteins are the most relevant factors that directly affect drug sensitivity. This is expected

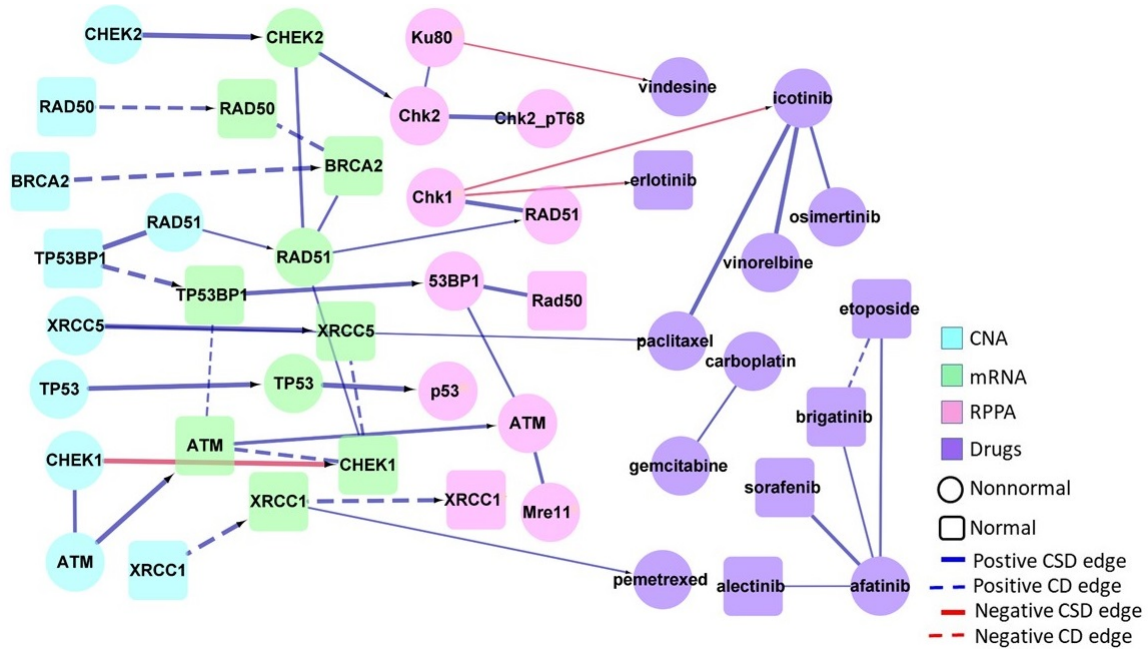


Figure 5: The estimated multilayered network for DNA Damage Response pathway. Blue and red edges indicate positive and negative dependencies, while CD and CSD stand for conditionally dependent and conditionally sign-dependent edges respectively. The width of the edges is proportional to the posterior inclusion probabilities.

as protein kinases serve as crucial targets for drug development (Davies et al., 2006). Proteins in the cell cycle pathway show the most connectivity with drugs across pathway-wise RPPA at 4 directed edges (Figure S.7). RPPA levels of Cyclin B1, E1 and E2 are found to regulate drug actions; these are cyclin-dependent kinase (CDK) inhibitors in the cell cycle that hold key significance in lung cancer cell proliferation (Baldi et al., 2011). Gemcitabine has the maximum number of connections with genomic platforms across drugs, with 3 edges from mRNA and RPPA of CAV1 in core and breast reactive pathways (Figure S.13 – S.14). Dependence of gemcitabine on CAV1 and its products has been explored in cell line studies and clinical trials which have shown that CAV1 over-expression can lead to gemcitabine-resistance in lung cancer cells (Ho et al., 2008; Shi et al., 2020).

5.2 Multilayered Pathway-level Networks

Inter-platform connectivity analysis from Figure 4 shows that the DNA damage response (DDR) pathway has the highest level of cross-platform signaling with drugs. Dysregulation of DDR promotes mutations that lead to chemotherapy resistance in lung cancer, and the understanding and characterization of inter- and intra- platform molecular mechanisms that affect drug sensitivity are crucial to the development of targeted therapies in lung cancer (Burgess et al., 2020). DDR molecular platforms are connected to drugs through 5 edges, with 1, 1, and 3 edges to drugs from CNA, mRNA and RPPA respectively (Figure 5). There are 10 and 6 edges respectively from CNA→mRNA and mRNA→RPPA, while no edges from CNA→RPPA. We observe negative dependencies of cell viability on protein levels of Checkpoint Kinase 1 (CHK1), the main effector of DDR, when cells are administered with EGFR TKIs erlotinib and icotinib, indicating high sensitivity of CHK1 toward these two drugs. Further, the CHK1 protein has a positive dependency with RAD51 protein expression which has cis-acting regulatory elements at the mRNA and CNA levels. Sensitivity towards pemetrexed and paclitaxel are found to be dependent on mRNA expressions of DNA repair genes XRCC1 and XRCC5, whose polymorphisms may affect DNA repair capacity and thus regulate cancer progression (Schneider et al., 2008).

Another interesting observation is on the positive dependencies between EGFR CNA, mRNA and protein levels and the sensitivity of EGFR CNA to osimertinib (Figure S.11). Higher levels of EGFR CNA are found to be associated with faster cell death when administered with osimertinib. EGFR sensitivity to osimertinib can be explained by clinical trials that show osimertinib successfully targets EGFR-mutant variants of NSCLC and shows improved efficacy over mutation-resistant standard EGFR-TKIs and platinum-based chemotherapies (Mok et al., 2017; Soria et al., 2018).

Several pairs of drug-drug dependencies appear in most of the pathways-level networks (Figure S.5). For instance, the positive dependency between EGFR-TKIs icotinib and

osimertinib is present in all the pathways. Both these drugs target EGFR, and are therefore expected to increase or decrease cell life span through similar patterns.

6 Discussion

In this article, we develop a multilayered network estimation framework, Robust Chain Graph Model (RCGM), to estimate and interpret directed and undirected edges in chain graphs under the presence of heavier-than-normal marginal tails. We incorporate the non-normality by proposing a random Gaussian-scale transformation of the original variables so that the transformed data is a Gaussian chain graph (GCM). The RCGM provides robust learning frameworks for various types of graphical models as special cases of chain graphs such as undirected networks by covariance/precision matrix specification and Bayesian networks when the entire topological order is known.

The increased scope of our model across heavy-tailed distributions comes at the expense of a Markov property weaker than conditional independence (CI), known as conditional sign-independence (CSI), to characterize dependencies for non-normal nodes. We assign each node a measure of its non-normality and use these scores to derive a probabilistic interpretation of CI and CSI properties. We incorporate sparsity in the chain graph by spike-and-slab priors on coefficients of the layer-wise regressions, and design the estimation algorithm to overcome the computational challenges that come with high-dimensional graphs using the node-wise likelihoods strategy (Ha et al., 2021). Furthermore, we show that our algorithm outperforms GCM methods in terms of graph structural recovery under various degrees of non-normality exhibited in the datasets.

From a scientific perspective, heterogeneity in drug responses, even for standard of care for different cancers including lung, demands genomic-based drug treatments developed by integrating molecular and clinical data across several biological domains. We perform integrative network analysis using our RCGM algorithm on genomic, transcriptomic, proteomic

and drug response data for lung cancer cell lines, available in the Cancer Dependency Map (www.depmap.org). We analyze the ways in which genomic features across key signaling pathways interact with each other and with mono-drug actions. From a global analysis of pathway-level networks, we identify pathways and genomic platforms most receptive to drugs. We find the DNA Damage Response (DDR) pathway to be the most connected with drugs and highlight its underlying dependencies.

In translational cancer research, diverse cancer models such as *in vivo* patient-derived xenografts (PDXs) have emerged as preclinical models that offer more faithful representation of genomic landscape of tumor and clinical outcomes than cancer cell lines (Gao et al., 2015; Woo et al., 2021). The growing number of PDX resources, e.g., PDXfinder, pdxfinder.org (Conte et al., 2019) have facilitated systematic identification and validation of druggable genomic events. The holistic characterization of information flow of relevant mechanisms of drug sensitivity and resistance in various model systems of human cancer can further the development of new targeted therapies including combination treatments. Our integrative analysis framework is expected to aid in the identification of key molecular processes that drive clinical outcomes across different cancer types and populations, which can further help in developing genomic testing-based precision medicine.

SUPPLEMENTARY MATERIAL

The Supplementary Material contains proofs of Theorem 2.1 and Corollary 2.2, details on the selection of mixing distributions, a description of MCMC sampling steps, and supplementary tables and figures. For reproducibility, the data and the R codes used for implementing our method are submitted with this paper.

FUNDING

MJH was supported by the National Institutes of Health grants R01CA244845-01A1 and R21CA22029, and start-up funds from University of Texas MD Anderson Cancer Center.

VB was supported by the National Institutes of Health grants R01-CA160736, R01CA244845-01A1, R21-CA220299, and P30 CA46592, US National Science Foundation grant 1463233, and start-up funds from the U-M Rogel Cancer Center and School of Public Health. AB was supported by US National Science Foundation Grant DMS-2014371.

References

- Akbani, R., Ng, P. K. S., Werner, H. M., Shahmoradgoli, M., Zhang, F., Ju, Z., Liu, W., Yang, J.-Y., Yoshihara, K., Li, J., et al. (2014). A pan-cancer proteomic perspective on the cancer genome atlas. *Nature Communications*, 5(1):1–15.
- Andersson, S. A., Madigan, D., and Perlman, M. D. (2001). Alternative Markov properties for chain graphs. *Scandinavian Journal of Statistics*, 28(1):33–85.
- Armstrong, H. J. (2005). *Bayesian estimation of decomposable Gaussian graphical models*. PhD thesis, University of New South Wales.
- Baldi, A., De Luca, A., Esposito, V., Campioni, M., Spugnini, E. P., and Citro, G. (2011). Tumor suppressors and cell-cycle proteins in lung cancer. *Pathology Research International*, 2011.
- Barretina, J., Caponigro, G., Stransky, N., Venkatesan, K., Margolin, A. A., Kim, S., Wilson, C. J., Lehár, J., Kryukov, G. V., Sonkin, D., et al. (2012). The cancer cell line encyclopedia enables predictive modelling of anticancer drug sensitivity. *Nature*, 483(7391):603–607.
- Bedard, P. L., Hansen, A. R., Ratain, M. J., and Siu, L. L. (2013). Tumour heterogeneity in the clinic. *Nature*, 501(7467):355–364.
- Bhadra, A. and Mallick, B. K. (2013). Joint high-dimensional Bayesian variable and covariance selection with an application to eqtl analysis. *Biometrics*, 69(2):447–457.

- Bhadra, A., Rao, A., and Baladandayuthapani, V. (2018). Inferring network structure in non-normal and mixed discrete-continuous genomic data. *Biometrics*, 74(1):185–195.
- Brambilla, E. and Gazdar, A. (2009). Pathogenesis of lung cancer signalling pathways: roadmap for therapies. *European Respiratory Journal*, 33(6):1485–1497.
- Burgess, J. T., Rose, M., Boucher, D., Plowman, J., Molloy, C., Fisher, M., O’leary, C., Richard, D. J., O’Byrne, K. J., and Bolderson, E. (2020). The therapeutic potential of dna damage repair pathways and genomic stability in lung cancer. *Frontiers in Oncology*, 10:1256.
- Chen, M., Ren, Z., Zhao, H., and Zhou, H. (2016). Asymptotically normal and efficient estimation of covariate-adjusted Gaussian graphical model. *Journal of the American Statistical Association*, 111(513):394–406.
- Conte, N., Mason, J. C., Halmagyi, C., Neuhauser, S., Mosaku, A., Yordanova, G., Chatzipi, A., Begley, D. A., Krupke, D. M., Parkinson, H., et al. (2019). Pdx finder: A portal for patient-derived tumor xenograft model discovery. *Nucleic Acids Research*, 47(D1):D1073–D1079.
- Corsello, S. M., Nagari, R. T., Spangler, R. D., Rossen, J., Kocak, M., Bryan, J. G., Humeidi, R., Peck, D., Wu, X., Tang, A. A., et al. (2020). Discovering the anticancer potential of non-oncology drugs by systematic viability profiling. *Nature Cancer*, 1(2):235–248.
- Davies, M., Hennessy, B., and Mills, G. B. (2006). Point mutations of protein kinases and individualised cancer therapy. *Expert Opinion on Pharmacotherapy*, 7(16):2243–2261.
- Dobra, A., Lenkoski, A., et al. (2011). Copula Gaussian graphical models and their applica-

- tion to modeling functional disability data. *The Annals of Applied Statistics*, 5(2A):969–993.
- Drton, M. and Eichler, M. (2006). Maximum likelihood estimation in Gaussian chain graph models under the alternative Markov property. *Scandinavian Journal of Statistics*, 33(2):247–257.
- Drton, M. and Perlman, M. D. (2008). A sinful approach to Gaussian graphical model selection. *Journal of Statistical Planning and Inference*, 138(4):1179–1200.
- Finegold, M. and Drton, M. (2011). Robust graphical modeling of gene networks using classical and alternative t -distributions. *The Annals of Applied Statistics*, pages 1057–1080.
- Finegold, M. and Drton, M. (2014). Robust Bayesian graphical modeling using Dirichlet t -distributions. *Bayesian Analysis*, 9(3):521–550.
- Friedman, J., Hastie, T., and Tibshirani, R. (2008). Sparse inverse covariance estimation with the graphical lasso. *Biostatistics*, 9(3):432–441.
- Gao, H., Korn, J. M., Ferretti, S., Monahan, J. E., Wang, Y., Singh, M., Zhang, C., Schnell, C., Yang, G., Zhang, Y., et al. (2015). High-throughput screening using patient-derived tumor xenografts to predict clinical trial drug response. *Nature medicine*, 21(11):1318–1325.
- Genest, C. and Nešlehová, J. G. (2014). Modeling dependence beyond correlation. In *Statistics in Action*, pages 83–102. Chapman and Hall/CRC.
- George, E. I. and McCulloch, R. E. (1993). Variable selection via Gibbs sampling. *Journal of the American Statistical Association*, 88(423):881–889.

- Ghandi, M., Huang, F. W., Jané-Valbuena, J., Kryukov, G. V., Lo, C. C., McDonald, E. R., Barretina, J., Gelfand, E. T., Bielski, C. M., Li, H., et al. (2019). Next-generation characterization of the cancer cell line encyclopedia. *Nature*, 569(7757):503–508.
- Gridelli, C., Morgillo, F., Favaretto, A., De Marinis, F., Chella, A., Cerea, G., Mattioli, R., Tortora, G., Rossi, A., Fasano, M., et al. (2011). Sorafenib in combination with erlotinib or with gemcitabine in elderly patients with advanced non-small-cell lung cancer: a randomized phase II study. *Annals of Oncology*, 22(7):1528–1534.
- Ha, M. J., Stingo, F. C., and Baladandayuthapani, V. (2021). Bayesian structure learning in multilayered genomic networks. *Journal of the American Statistical Association*, 116(534):605–618.
- Ho, C.-C., Kuo, S.-H., Huang, P.-H., Huang, H.-Y., Yang, C.-H., and Yang, P.-C. (2008). Caveolin-1 expression is significantly associated with drug resistance and poor prognosis in advanced non-small cell lung cancer patients treated with gemcitabine-based chemotherapy. *Lung Cancer*, 59(1):105–110.
- Iorio, F., Knijnenburg, T. A., Vis, D. J., Bignell, G. R., Menden, M. P., Schubert, M., Aben, N., Gonçalves, E., Barthorpe, S., Lightfoot, H., et al. (2016). A landscape of pharmacogenomic interactions in cancer. *Cell*, 166(3):740–754.
- Kasarskis, A., Yang, X., and Schadt, E. (2011). Integrative genomics strategies to elucidate the complexity of drug response. *Pharmacogenomics*, 12(12):1695–1715.
- Langer, C. J., Leighton, J. C., Comis, R. L., O’Dwyer, P. J., McAleer, C. A., Bonjo, C. A., Engstrom, P. F., Litwin, S., and Ozols, R. F. (1995). Paclitaxel and carboplatin in combination in the treatment of advanced non-small-cell lung cancer: a phase ii toxicity, response, and survival analysis. *Journal of Clinical Oncology*, 13(8):1860–1870.

- Lauritzen, S. L. (1996). *Graphical models*, volume 17. Clarendon Press.
- Li, Y., Datta, J., Craig, B. A., and Bhadra, A. (2021). Joint mean–covariance estimation via the horseshoe. *Journal of Multivariate Analysis*, 183:104716.
- Liang, H., Wang, H. B., Liu, H. Z., Wen, X. J., Zhou, Q. L., and Yang, C. X. (2013). The effects of combined treatment with sevoflurane and cisplatin on growth and invasion of human adenocarcinoma cell line a549. *Biomedicine & Pharmacotherapy*, 67(6):503–509.
- Lim, Z.-F. and Ma, P. C. (2019). Emerging insights of tumor heterogeneity and drug resistance mechanisms in lung cancer targeted therapy. *Journal of Hematology and Oncology*, 12(1):1–18.
- Lin, J., Basu, S., Banerjee, M., and Michailidis, G. (2016). Penalized maximum likelihood estimation of multi-layered Gaussian graphical models. *Journal of Machine Learning Research*, 17(146):1–51.
- Liu, H., Han, F., Yuan, M., Lafferty, J., and Wasserman, L. (2012). High-dimensional semiparametric Gaussian copula graphical models. *The Annals of Statistics*, 40(4):2293–2326.
- Liu, H., Lafferty, J., and Wasserman, L. (2009). The nonparanormal: Semiparametric estimation of high dimensional undirected graphs. *Journal of Machine Learning Research*, 10(10).
- McCarter, C. and Kim, S. (2014). On sparse Gaussian chain graph models. *Advances in Neural Information Processing Systems*, 27:3212–3220.
- Mok, T. S., Wu, Y.-L., Ahn, M.-J., Garassino, M. C., Kim, H. R., Ramalingam, S. S., Shepherd, F. A., He, Y., Akamatsu, H., Theelen, W. S., et al. (2017). Osimertinib

- or platinum–pemetrexed in egfr t790m–positive lung cancer. *New England Journal of Medicine*, 376(7):629–640.
- Morris, J. S. and Baladandayuthapani, V. (2017). Statistical contributions to bioinformatics: Design, modelling, structure learning and integration. *Statistical Modelling*, 17(4-5):245–289.
- Nelsen, R. B. (2007). *An Introduction to Copulas*. Springer Science & Business Media.
- Petersen, L. (2018). Sparse learning in Gaussian chain graphs for state space models. In *International Conference on Probabilistic Graphical Models*, pages 332–343. PMLR.
- Pitt, M., Chan, D., and Kohn, R. (2006). Efficient Bayesian inference for Gaussian copula regression models. *Biometrika*, 93(3):537–554.
- Robichaux, J. P., Le, X., Vijayan, R., Hicks, J. K., Heeke, S., Elamin, Y. Y., Lin, H. Y., Udagawa, H., Skoulidis, F., Tran, H., et al. (2021). Structure-based classification predicts drug response in egfr-mutant nscl. *Nature*, 597(7878):732–737.
- Roden, D. M., McLeod, H. L., Relling, M. V., Williams, M. S., Mensah, G. A., Peterson, J. F., and Driest, S. L. V. (2019). Pharmacogenomics. *The Lancet*, 394(10197):521–532.
- Rothman, A. J., Levina, E., and Zhu, J. (2010). Sparse multivariate regression with covariance estimation. *Journal of Computational and Graphical Statistics*, 19(4):947–962.
- Schneider, J., Classen, V., and Helmig, S. (2008). Xrcc1 polymorphism and lung cancer risk. *Expert review of molecular diagnostics*, 8(6):761–780.
- Shi, Y.-B., Li, J., Lai, X.-N., Jiang, R., Zhao, R.-C., and Xiong, L.-X. (2020). Multifaceted roles of caveolin-1 in lung cancer: a new investigation focused on tumor occurrence, development and therapy. *Cancers*, 12(2):291.

- Soria, J.-C., Ohe, Y., Vansteenkiste, J., Reungwetwattana, T., Chewaskulyong, B., Lee, K. H., Dechaphunkul, A., Imamura, F., Nogami, N., Kurata, T., et al. (2018). Osimertinib in untreated egfr-mutated advanced non-small-cell lung cancer. *New England Journal of Medicine*, 378(2):113–125.
- Squassina, A., Manchia, M., Manolopoulos, V. G., Artac, M., Lappa-Manakou, C., Karkabouna, S., Mitropoulos, K., Zompo, M. D., and Patrinos, G. P. (2010). Realities and expectations of pharmacogenomics and personalized medicine: impact of translating genetic knowledge into clinical practice. *Pharmacogenomics*, 11(8):1149–1167.
- Vicent, S., Garayoa, M., López-Picazo, J. M., Lozano, M. D., Toledo, G., Thunnissen, F. B., Manzano, R. G., and Montuenga, L. M. (2004). Mitogen-activated protein kinase phosphatase-1 is overexpressed in non-small cell lung cancer and is an independent predictor of outcome in patients. *Clinical Cancer Research*, 10(11):3639–3649.
- Vogelstein, B. and Kinzler, K. W. (2004). Cancer genes and the pathways they control. *Nature Medicine*, 10(8):789–799.
- Woo, X. Y., Giordano, J., Srivastava, A., Zhao, Z.-M., Lloyd, M. W., de Bruijn, R., Suh, Y.-S., Patidar, R., Chen, L., Scherer, S., et al. (2021). Conservation of copy number profiles during engraftment and passaging of patient-derived cancer xenografts. *Nature genetics*, 53(1):86–99.
- Xue, L. and Zou, H. (2012). Regularized rank-based estimation of high-dimensional non-paranormal graphical models. *The Annals of Statistics*, 40(5):2541–2571.
- Yin, J. and Li, H. (2011). A sparse conditional Gaussian graphical model for analysis of genetical genomics data. *The Annals of Applied Statistics*, 5(4):2630.

Supplementary Materials for

Bayesian Robust Learning in Chain Graph Models for Integrative Pharmacogenomics

S.1 Proofs

This section consists of the proofs of Theorem 2.1 and Corollary 2.2. We adapt the proof of Proposition 1 of Bhadra et al. (2018) to our chain graph context.

S.1.1 Proof of Theorem 2.1 (i)

(a) Let $\mathcal{L}(u) = \mathcal{L}(v) = l$. Let pa_l be the indices of nodes in layers $1 : (l-1)$. By construction of the non-normal chain graph model in (2), \mathbf{X}_l given \mathbf{D} and \mathbf{X}_{pa_l} can be written as

$$\mathbf{D}_l \mathbf{X}_l | \mathbf{X}_{\text{pa}_l}, \mathbf{D} \sim N(\mathbf{B}_{l, \text{pa}_l} \mathbf{D}_{\text{pa}_l} \mathbf{X}_{\text{pa}_l}, \mathcal{K}_l^{-1}).$$

Let \mathbf{g}_l be equal to $\mathbf{B}_{l, \text{pa}_l} \mathbf{D}_{\text{pa}_l} \mathbf{X}_{\text{pa}_l}$, so that $E(\mathbf{D}_l \mathbf{X}_l | \mathbf{X}_{\text{pa}_l}, \mathbf{D}) = \mathbf{g}_l$. Note that \mathbf{g}_l is free of \mathbf{X}_l and \mathbf{D}_l . Also, let $\mathbf{g}_l = ((g))_j, j \in \mathcal{T}_l$. By properties of the multivariate normal distribution,

$$\left(\frac{X_u}{d_u}, \frac{X_v}{d_v} \right) | \mathbf{X}_{[1:l] \setminus \{u,v\}}, \mathbf{D} \sim N_2 \left(\left(\begin{array}{c} \mu_{uD} \\ \mu_{vD} \end{array} \right), \mathcal{K}_{\{u,v\}}^{-1} \right), \quad (\text{S.1})$$

where $\mu_{jD} = E(X_j/d_j | \mathbf{X}_{[1:l] \setminus \{u,v\}}, \mathbf{D})$, $j = u, v$, and

$$\mathcal{K}_{\{u,v\}} = \begin{pmatrix} k_{uu} & k_{uv} \\ k_{vu} & k_{vv} \end{pmatrix}.$$

When $k_{uv} = 0$, the joint conditional likelihood factorizes into the product of the individual conditional likelihoods, so that

$$f\left(\frac{X_u}{d_u}, \frac{X_v}{d_v} \middle| \mathbf{X}_{[1:l]\setminus\{u,v\}}, \mathbf{D}\right) = \left(\frac{1}{\sqrt{2\pi}}\right)^2 k_{uu}^{1/2} \exp\left(-\frac{1}{2}\left(\frac{X_u}{d_u} - \mu_{u\mathbf{D}}\right)^T k_{uu} \left(\frac{X_u}{d_u} - \mu_{u\mathbf{D}}\right)\right) \\ k_{vv}^{1/2} \exp\left(-\frac{1}{2}\left(\frac{X_v}{d_v} - \mu_{v\mathbf{D}}\right)^T k_{vv} \left(\frac{X_v}{d_v} - \mu_{v\mathbf{D}}\right)\right). \quad (\text{S.2})$$

From Proposition C.5 of Lauritzen (1996), $\mu_{j\mathbf{D}} = E(X_j/d_j | \mathbf{X}_{[1:l]\setminus\{u,v\}}, \mathbf{D})$, $j = u, v$, can be deduced as

$$\mu_{j\mathbf{D}} = g_j - \frac{1}{k_{jj}} \sum_{t \neq u, v; t \in \mathcal{T}_l} k_{jt} \left(\frac{X_t}{d_t} - g_t\right), \quad j = u, v.$$

From (S.2), (X_u/d_u) and (X_v/d_v) are conditionally independent given $(\mathbf{X}_{[1:l]\setminus\{u,v\}}, \mathbf{D})$. Therefore, when $k_{uv} = 0$, $(Y_j/d_j) | \mathbf{X}_{[1:l]\setminus\{u,v\}}, \mathbf{D} \sim N(\mu_{j\mathbf{D}}, k_{jj}^{-1})$, $j = u, v$. For the rest of the proof of part (i), we prove results involving X_u . The corresponding results for X_v follow in an exact similar way. We evaluate

$$\begin{aligned} \text{P}(X_u < 0 | \mathbf{X}_{[1:l]\setminus\{u,v\}}, \mathbf{D}) &= \text{P}\left(\frac{X_u}{d_u} < 0 \middle| \mathbf{X}_{[1:l]\setminus\{u,v\}}, \mathbf{D}\right) \\ &= \text{P}\left(k_{uu}^{1/2} \left(\frac{X_u}{d_u} - \mu_{u\mathbf{D}}\right) < -k_{uu}^{1/2} \mu_{u\mathbf{D}} \middle| \mathbf{X}_{[1:l]\setminus\{u,v\}}, \mathbf{D}\right) \\ &= \Phi(-k_{uu}^{1/2} \mu_{u\mathbf{D}}). \end{aligned} \quad (\text{S.3})$$

Note that since $\mu_{u\mathbf{D}}$ is free of (X_u, X_v, d_u, d_v) , the RHS of (S.3) is free of those as well. Similar calculation follows for X_v , so that $\text{P}(X_v < 0 | \mathbf{X}_{[1:l]\setminus\{u,v\}}, \mathbf{D}) = \Phi(-k_{vv}^{1/2} \mu_{v\mathbf{D}})$.

Next, by properties of multivariate normal distribution, we have that

$$(X_u/d_u) | \mathbf{X}_{[1:l]\setminus\{u\}}, \mathbf{D} \sim N(\tilde{\mu}_{u\mathbf{D}}, k_{uu}^{-1}),$$

where

$$\tilde{\mu}_{u\mathbf{D}} = g_u - \frac{1}{k_{uu}} \sum_{t \neq u} k_{ut} \left(\frac{X_t}{d_t} - g_t \right).$$

Then it follows that

$$\begin{aligned} \mathrm{P}(X_u < 0 | \mathbf{X}_{[1:l] \setminus \{u\}}, \mathbf{D}) &= \mathrm{P} \left(\frac{X_u}{d_u} < 0 | \mathbf{X}_{[1:l] \setminus \{u\}}, \mathbf{D} \right) \\ &= \mathrm{P} \left(k_{uu}^{1/2} \left(\frac{X_u}{d_u} - \tilde{\mu}_{u\mathbf{D}} \right) < -k_{uu}^{1/2} \tilde{\mu}_{u\mathbf{D}} | \mathbf{X}_{[1:l] \setminus \{u\}}, \mathbf{D} \right) \\ &= \Phi(-k_{uu}^{1/2} \tilde{\mu}_{u\mathbf{D}}). \end{aligned} \quad (\text{S.4})$$

When $k_{uv} = 0$, the term corresponding to $t = v$ in the expression of $\tilde{\mu}_{u\mathbf{D}}$ vanishes, so that

$$\tilde{\mu}_{u\mathbf{D}} = \mu_{u\mathbf{D}}.$$

Therefore, when $k_{uv} = 0$, (S.3) and (S.4) are equal, so that $\mathrm{P}(X_u < 0 | \mathbf{X}_{[1:l] \setminus \{u,v\}}, \mathbf{D})$ is equal to $\mathrm{P}(X_u < 0 | \mathbf{X}_{[1:l] \setminus \{u\}}, \mathbf{D})$.

Now note that the conditional likelihood of $\mathbf{D}\mathbf{X}$ given \mathbf{D} factorizes in terms of d_v 's, and $d_v \sim p_v$ are chosen independent of each other. Therefore $\pi(\mathbf{D}|\mathbf{X})$ factorizes into the product of $\pi(1/d_v|X_v)$. Using this fact, we evaluate

$$\begin{aligned} \mathrm{P}(X_u < 0 | \mathbf{X}_{[1:l] \setminus \{u,v\}}) &= \int \mathrm{P}(X_u < 0 | \mathbf{X}_{[1:l] \setminus \{u,v\}}, \mathbf{D}_{[1:l]}) d\pi(\mathbf{D}_{[1:l]} | \mathbf{X}_{[1:l] \setminus \{u,v\}}) \\ &= \int \mathrm{P}(X_u < 0 | \mathbf{X}_{[1:l] \setminus \{u\}}, \mathbf{D}_{[1:l]}) d\pi(\mathbf{D}_{[1:l] \setminus \{u,v\}} | \mathbf{X}_{[1:l] \setminus \{u,v\}}) \\ &= \int \mathrm{P}(X_u < 0 | \mathbf{X}_{[1:l] \setminus \{u\}}, \mathbf{D}_{[1:l]}) \left(\int d\pi(d_v^{-1} | \mathbf{X}_{[1:l] \setminus \{u,v\}}) \right) \\ &\quad d\pi(\mathbf{D}_{[1:l] \setminus \{u,v\}} | \mathbf{X}_{[1:l] \setminus \{u,v\}}) \\ &= \int \mathrm{P}(X_u < 0 | \mathbf{X}_{[1:l] \setminus \{u\}}, \mathbf{D}_{[1:l]}) d\pi(\mathbf{D}_{[1:l] \setminus u} | \mathbf{X}_{[1:l] \setminus \{u\}}) \\ &= \int \mathrm{P}(X_u < 0 | \mathbf{X}_{[1:l] \setminus \{u\}}, \mathbf{D}_{[1:l]}) d\pi(\mathbf{D}_{[1:l]} | \mathbf{X}_{[1:l] \setminus \{u\}}) \end{aligned}$$

$$= \text{P}(X_u < 0 | \mathbf{X}_{[1:l] \setminus \{u\}}). \quad (\text{S.5})$$

The swapping of integrals is ensured by Fubini's theorem which can be applied here as $0 < d_u < \infty$ and $\int p_u(d_u) < \infty$ by assumption on d_v s.

(b) Let $\mathcal{L}(u) < \mathcal{L}(v)$ and $\mathcal{L}(v) = l$. Note that $\mathbf{X}_{\{v\} \cup [1:l-1]} \mathbf{D}_{\{v\} \cup [1:l-1]} | \mathbf{D}$ follows a multivariate normal distribution. We then have,

$$\left(\frac{X_u}{d_u}, \frac{X_v}{d_v} \right) | \mathbf{X}_{[1:l-1] \setminus \{u\}}, \mathbf{D} \sim N_2 \left(\begin{pmatrix} \mu_{u\mathbf{D}} \\ \mu_{v\mathbf{D}} \end{pmatrix}, \mathcal{K}_{\{u,v\}}^{-1} \right),$$

where $\mu_{j\mathbf{D}} = E(X_j/d_j | \mathbf{X}_{[1:l-1] \setminus \{u\}}, \mathbf{D})$, $j = u, v$. Therefore,

$$(X_j/d_j) | \mathbf{X}_{[1:l-1] \setminus \{u\}}, \mathbf{D} \sim N(\mu_{j\mathbf{D}}, k_{jj}^{-1}).$$

Also, for $j = u, v$,

$$(X_j/d_j) | \mathbf{X}_{[\{v\} \cup [1:l-1]] \setminus \{j\}}, \mathbf{D} \sim N(\tilde{\mu}_{j\mathbf{D}}, k_{jj}^{-1}),$$

where $\tilde{\mu}_{j\mathbf{D}} = E(X_j/d_j | \mathbf{X}_{[\{v\} \cup [1:l-1]] \setminus \{j\}}, \mathbf{D})$.

Therefore, for $j = u, v$,

$$\begin{aligned} \text{P}(X_j < 0 | \mathbf{X}_{[1:l-1] \setminus \{u\}}, \mathbf{D}) &= \text{P} \left(\frac{X_j}{d_j} < 0 | \mathbf{X}_{[1:l-1] \setminus \{u\}}, \mathbf{D} \right) \\ &= \text{P} \left(k_{jj}^{1/2} \left(\frac{X_j}{d_j} - \mu_{j\mathbf{D}} \right) < -k_{jj}^{1/2} \mu_{j\mathbf{D}} \mid \mathbf{X}_{[1:l-1] \setminus \{u\}}, \mathbf{D} \right) \\ &= \Phi(-k_{jj}^{1/2} \mu_{j\mathbf{D}}). \end{aligned} \quad (\text{S.6})$$

Also,

$$\text{P}(X_j < 0 | \mathbf{X}_{[\{v\} \cup [1:l-1]] \setminus \{j\}}, \mathbf{D}) = \text{P} \left(\frac{X_j}{d_j} < 0 | \mathbf{X}_{[\{v\} \cup [1:l-1]] \setminus \{j\}}, \mathbf{D} \right)$$

$$\begin{aligned}
&= \mathbb{P} \left(k_{jj}^{1/2} \left(\frac{X_j}{d_j} - \tilde{\mu}_{j\mathbf{D}} \right) < -k_{jj}^{1/2} \tilde{\mu}_{j\mathbf{D}} \mid \mathbf{X}_{\{\{v\} \cup [1:l-1]\} \setminus \{j\}}, \mathbf{D} \right) \\
&= \Phi(-k_{jj}^{1/2} \tilde{\mu}_{j\mathbf{D}}). \tag{S.7}
\end{aligned}$$

We now show that $\mu_{u\mathbf{D}} = \tilde{\mu}_{v\mathbf{D}}$ when $\mathbf{B}_{vu} = 0$. To show this, note that

$$\begin{aligned}
\mathbb{E}(X_v/d_v \mid \mathbf{X}_{[1:l-1]}, \mathbf{D}) &= \mathbf{B}_{v,[1:l-1]} \mathbf{D}_{[1:l-1]} \mathbf{X}_{[1:l-1]} \\
&= \sum_{t \in [1:l-1]} \frac{\mathbf{B}_{vt} X_t}{d_t} \\
&= \sum_{t \in [1:l-1] \setminus \{u\}} \frac{\mathbf{B}_{vt} X_t}{d_t} \\
&= \mathbb{E}(X_v/d_v \mid \mathbf{X}_{[1:l-1] \setminus \{u\}}, \mathbf{D}).
\end{aligned}$$

Now note that since $\mathbf{B}_{vu} = 0$, the construction of the chain graph (Equation (2)) implies that $\mathbf{B}_{uv} = 0$. Therefore it follows from the last display that $\mathbb{E}(X_u/d_u \mid \mathbf{X}_{[1:l-1] \setminus \{u\}}, \mathbf{D}) = \mathbb{E}(X_u/d_u \mid \mathbf{X}_{\{v\} \cup [1:l-1] \setminus \{u\}}, \mathbf{D})$.

Therefore, when $\mathbf{B}_{vu} = 0$, $\tilde{\mu}_{j\mathbf{D}} = \mu_{j\mathbf{D}}$ for $j = u, v$, so that $\mathbb{P}(X_j < 0 \mid \mathbf{X}_{[1:l-1] \setminus \{u\}}, \mathbf{D})$ is equal to $\mathbb{P}(X_j < 0 \mid \mathbf{X}_{\{\{v\} \cup [1:l-1]\} \setminus \{j\}}, \mathbf{D})$. The rest of the proof involves integrating out \mathbf{D} and follows similar to Equation (S.5).

S.1.2 Proof of Theorem 2.1 (ii)

We prove the result for undirected edges. From (S.2), we have that (X_u/d_u) and (X_v/d_v) given $(\mathbf{X}_{[1:l] \setminus \{u,v\}}, \mathbf{D})$ are jointly bivariate normal and are independent, so that

$$f(X_u/d_u \mid \mathbf{X}_{[1:l] \setminus \{u,v\}}, \mathbf{D}) = f(X_u/d_u \mid \mathbf{X}_{[1:l] \setminus \{u\}}, \mathbf{D}),$$

when $k_{uv} = 0$. We then have

$$\begin{aligned}
f(X_u | \mathbf{X}_{[1:l] \setminus \{u,v\}}) &= \int f(X_u | \mathbf{X}_{[1:l] \setminus \{u,v\}}, \mathbf{D}_{[1:l]}) d\pi(\mathbf{D}_{[1:l] \setminus u} | \mathbf{X}_{[1:l] \setminus \{u,v\}}) \\
&= \int d_u^{-1} f(X_u/d_u | \mathbf{X}_{[1:l] \setminus \{u,v\}}, \mathbf{D}_{[1:l]}) d\pi(\mathbf{D}_{[1:l] \setminus u} | \mathbf{X}_{[1:l] \setminus \{u,v\}}) \\
&= \int d_u^{-1} f(X_u/d_u | \mathbf{X}_{[1:l] \setminus \{u\}}, \mathbf{D}_{[1:l]}) d\pi(\mathbf{D}_{[1:l] \setminus u} | \mathbf{X}_{[1:l] \setminus \{u\}}) \\
&= \int f(X_u | \mathbf{X}_{[1:l] \setminus \{u\}}, \mathbf{D}_{[1:l]}) d\pi(\mathbf{D}_{[1:l] \setminus u} | \mathbf{X}_{[1:l] \setminus \{u\}}) \\
&= f(X_u | \mathbf{X}_{[1:l] \setminus \{u\}}). \tag{S.8}
\end{aligned}$$

The interchange of integrals in $d\pi(\mathbf{D})$ in the last display follows from arguments similar to (S.5). The relation in Equation (S.2) also holds when $\mathcal{L}(u) < \mathcal{L}(v)$ and $\mathbf{B}_{vu} = 0$, so the proof in this case would follow similar to the last two displays.

S.1.3 Proof of Corollary 2.2

Let $\mathcal{L}(u) = \mathcal{L}(v) = l$. Let H_1 denote the event of conditional sign independence:

$$H_1 = \{P(X_u < 0 | \mathbf{X}_{[1:l] \setminus \{u,v\}}) = P(X_u < 0 | \mathbf{X}_{[1:l] \setminus u})\}.$$

Then $P(H_1) = \sum_{\omega_u, \omega_v} P(H_1 | \omega_u, \omega_v) P(\omega_u, \omega_v)$, where ω_u, ω_v are 0 or 1. From part (i) of Theorem 2.1, H_1 is true whenever at least one of ω_u, ω_v is 1. From part (ii) of Theorem 2.1, conditional independence is observed when $\omega_u = \omega_v = 0$. As conditional sign independence is a weaker property, it is observed when $\omega_u = \omega_v = 0$. So when $k_{uv} = 0$,

$$\begin{aligned}
P(H_1 | \omega_u = 1, \omega_v = 1) &= P(H_1 | \omega_u = 1, \omega_v = 0) = P(H_1 | \omega_u = 0, \omega_v = 1) \\
&= P(H_1 | \omega_u = 0, \omega_v = 0) = 1,
\end{aligned}$$

so that $P(H_1) = 1$.

For conditional independence, let H_2 denote the event:

$$H_2 = \{f(X_u | \mathbf{X}_{[1:l] \setminus \{u,v\}}) = f(X_u | \mathbf{X}_{[1:l] \setminus \{u\}})\}.$$

Then

$$\begin{aligned} P(H_2) &= \sum_{\omega_u, \omega_v} P(H_2 | \omega_u, \omega_v) P(\omega_u, \omega_v) \\ &\geq P(H_2 | \omega_u = \omega_v = 0) P(\omega_u = 0, \omega_v = 0). \end{aligned}$$

From part (ii) of Theorem 2.1, $P(H_2 | \omega_u = \omega_v = 0) = 1$. As $\omega_v \sim \text{Bern}(\pi_v)$ independently, $P(\omega_u = 0, \omega_v = 0) = 1 - \pi_u - \pi_v + \pi_u \pi_v$. Therefore $P(H_2) = 1 - \pi_u - \pi_v + \pi_u \pi_v$. Similar calculations would follow for X_v , and for $\mathcal{L}(u) < \mathcal{L}(v)$.

S.2 Node-wise Likelihood Equations

For a node v belonging to layer l , let \mathbf{b}_v be the entries in the row of \mathbf{B}_l corresponding to v , with $\mathbf{b}_v = \mathbf{0}$ if $l = 1$. Let $\mathbf{a}_v = -k_{vv}^{-1} \mathbf{k}_l^{(v)}$, where $\mathbf{k}_l^{(v)}$ is the vector of k_{vu} , $u \in \mathcal{T}_l \setminus v$. We reparameterize the precision parameters to regression coefficients on residuals after taking out the effects of previous layers, so that given \mathbf{D} , we have

$$(X_v/d_v) = (\mathbf{X}\mathbf{D})_{[1:\mathcal{L}(v)-1]}^T \mathbf{b}_v + \epsilon_v,$$

where $\boldsymbol{\epsilon} = (\epsilon_1, \dots, \epsilon_q)$, $\epsilon_v = \boldsymbol{\epsilon}_{\mathcal{T}_l \setminus v}^T \mathbf{a}_v + e_v$, and $e_v \sim N(0, k_{vv}^{-1})$ is independent of $\boldsymbol{\epsilon}_{V \setminus v}$. Let $\mathbf{B}_l^{(v)}$ be the submatrix of \mathbf{B}_l consisting of all but the row corresponding to the node v . Applying the node-wise regression in Proposition 1 in Ha et al. (2021), for the scaled

random variables given \mathbf{D} , we have the node-conditional equation

$$\frac{X_v}{d_v} = (\mathbf{X}\mathbf{D})_{[1:l-1]}^T (\mathbf{b}_v - \mathbf{B}_l^{(v)} \mathbf{a}_v) + (\mathbf{X}\mathbf{D})_{\mathcal{T}_l \setminus v}^T \mathbf{a}_v + e_v.$$

With the identifiability constraints imposed, given \mathbf{D} , the v -th node-conditional regression is of the form

$$(X_v/d_v) = (\mathbf{X}\mathbf{D})_{[1:l-1]}^T \mathbf{b}_v + \boldsymbol{\epsilon}_{\mathcal{T}_l \setminus v}^T \mathbf{a}_v + e_v,$$

where $\boldsymbol{\epsilon}_{\mathcal{T}_l \setminus v}^T = (\mathbf{X}\mathbf{D})_{\mathcal{T}_l \setminus v}^T - (\mathbf{X}\mathbf{D})_{[1:l-1]}^T \mathbf{B}_l^{(v)}$ is assumed fixed given \mathbf{D} . We reparameterize \mathbf{a}_v , \mathbf{b}_v , k_{vv} for every $v \in V$ and $\mathcal{L}(v) = l$, to obtain the layer-wise estimates of \mathbf{B} and \mathcal{K} as

$$\begin{aligned} ((\mathbf{B}_l))_{vu} &= \mathbf{b}_{vu}, \\ ((\mathcal{K}_l))_{vu} &= -k_{vv} a_{vu}, \quad u \in \mathcal{T}_l \setminus v. \end{aligned} \tag{S.9}$$

S.3 Identifiability in Node-wise Likelihood Equation

Throughout this section, let $\mathbf{Y} = \mathbf{D}\mathbf{X}$ denote the scaled data. Let us examine a simple case of the model as described in Figure S.1. The node-wise equation for Y_3 would be

$$Y_3 = (b_{31}Y_1 + b_{32}Y_2) + a_{34}Y_4 - a_{34}b_{42}Y_2.$$

From the figure, it appears that $b_{32} = 0$, but b_{32} would still appear in the node-wise regression equation. The previous equation can be re-written as

$$Y_3 = b_{31}Y_1 + (b_{32} - a_{34}b_{42})Y_2 + a_{34}Y_4.$$

Now let \hat{b} be the estimated coefficient for Y_2 . We assume a_{34} known when estimating b , so $\hat{b} = b_{32} - a_{34}b_{42}$ is one equation with two variables b_{32} and b_{42} which cannot be solved uniquely. As an example, consider the two different sets of solutions:

1. $(b_{32} = 0, b_{42} = -\hat{b}/a_{34})$: graph on the left panel. There is no edge between Y_3 and Y_2 .
2. $(b_{32} = \hat{b}, b_{42} = 0)$: graph on the right panel. There is no edge between Y_4 and Y_2 .



Figure S.1: An example demonstrating the node-wise regressions for a two-layer chain graph with two nodes in each layer

In this example, it is not possible to identify whether the effect of Y_2 on Y_3 is through the directed edge b_{32} or via the indirect effect of Y_4 (through $a_{34}b_{42}$). So the identifiability problem can potentially lead to inconsistent edge detection.

S.4 Selection of Mixing Distributions

If v is a node with heavy tails such that $\omega_v = 1$, then

$$\begin{aligned}
 d_v | (\omega_v = 1) &\sim p_v, \\
 f(X_v | \omega_v = 1) &= \int d_v^{-1} \phi(X_v/d_v) dp_v(d_v),
 \end{aligned}
 \tag{S.10}$$

Algorithm 2: Selection of mixing distribution p_v 's

Given the multivariate data \mathbf{X} with q coordinates,;
while $1 \leq i \leq q$ **do**
 Let $\mathbf{x} = [\mathbf{X}_v - \text{mean}(\mathbf{X}_v)]/\text{s.d.}(X_v)$;
 (**double-exponential fitting**). Evaluate p_e , the p -value of the regression
 $\log \hat{f}(x) = a_0 + a_1 \log |x| + a_2 |x|$.;
 (**t-distribution fitting**). Evaluate p_t , the p -value of the regression
 $\log \hat{f}(x) = a_0 + a_2 |x|$.;
 (**select category and parameters of p_v**). **if** $p_e < p_t$ **then**
 | Set p_v as Gamma(shape= $(a_1 + 1)/2$, scale= $a_1^2/2$)
 end
 else
 | Set p_v as Inverse-Gamma(shape= $(-a_1 + 1)/2$, scale= $(-a_1 + 1)/2$)
 end
end

where $\phi(\cdot)$ is the pdf of a standard normal distribution. From Lemma 1 of Bhadra et al. (2018), if the tail of \mathbf{X}_v decays polynomially as $\alpha|x|^{2\lambda\nu-1}$ for some $\lambda \leq 0$, $\nu \in \mathbb{R}$, $\alpha \in (0, 1)$ then the mixing density p_v has the right-tail decaying as $\alpha d_v^{\lambda\nu-1}$. Further, if the marginal decays exponentially as $|x|^{2\lambda\nu-1} \exp\{-(2\psi\nu)^{1/2}|x|\}$ for $\lambda \in \mathbb{R}$ and $\psi > 0$, then p_v has tail decaying as $d_v^{\lambda\nu-1} \exp(-\psi\nu d_v)$. So the rate of decay in marginal tails can be directly used to set the parameters of the mixing distribution p_v . Algorithm 2 describes the procedure for setting the tail parameters of p_v .

S.5 MCMC Sampling Steps Summary

We first choose p_v for each node v using Algorithm 2. We then set the prior of π_v as Beta($\mu_v r_v, (1 - \mu_v) r_v$), where $\mu_v = H(\mathbf{x}_v)$, $H(\mathbf{x}_v) = 2 * \Phi(\log(1 - pval(\mathbf{x}_v)))$, with Φ and $pval$ respectively being the cdf of standard normal distribution and the p -value of the Kolmogorov-Smirnov test for normality, $r_v = [\mu_v(1 - \mu_v)/\xi_v] - 1$, with the prior variance ξ_v set to 0.01 if $s_v > 0.01$ and $0.01s_v$ otherwise, for $s_v = \mu_v(1 - \mu_v)$. We center and scale each

coordinate of \mathbf{X} before computation. At iteration t of the MCMC sampling, we generate \mathbf{D} for every subject i given current $\boldsymbol{\pi}$ as $d_{iv} \sim \pi_v p_v + (1 - \pi_v)\delta_1$ for all $v \in V$. We then accept the sampled d_{iv} based on the ratio

$$R = \frac{\phi(X_{iv}d_{iv})p_v(d_{iv}^*)}{\phi(X_{iv}d_{iv}^*)p_v(d_{iv})}, \quad (\text{S.11})$$

where d_{iv}^* is the current value of d_{iv} and ϕ is the density of a standard normal distribution. We accept d_{iv} if $U \sim \text{Unif}(0, 1)$ is less than R . Next, for every layer l , we update the normality measures and directed and undirected edges as described below.

To update the non-normality measure $\boldsymbol{\pi}$, let $\boldsymbol{\pi}^s$ be the current state of $\boldsymbol{\pi}$. We generate the new sample $\boldsymbol{\pi}^*$ by generating π_v^* for every $v \in \mathcal{T}_l$ from $\text{Beta}(\xi_v^0(\xi_v^0/r_v^2 - 1), (1 - \xi_v^0)(\xi_v^0/r_v^2 - 1))$. For every $v \in \mathcal{T}_l$, we look at the acceptance ratio

$$R = \frac{[\pi_v^* \phi(\tilde{\mathbf{X}}_v/d_v | \mu_v^D, \boldsymbol{\pi}^*, k_{vv})p_v(d_v) + (1 - \pi_v^*) \phi(\tilde{\mathbf{X}}_v | \mu_v, \boldsymbol{\pi}^*, k_{vv})]g(\pi_v^*)}{[\pi_v^s \phi(\tilde{\mathbf{X}}_v/d_v | \mu_v^D, \boldsymbol{\pi}^s, k_{vv})p_v(d_v) + (1 - \pi_v^s) \phi(\tilde{\mathbf{X}}_v | \mu_v, \boldsymbol{\pi}^s, k_{vv})]g(\pi_v^s)}, \quad (\text{S.12})$$

where g is the density function of $\text{Beta}(\xi_v^0(\xi_v^0/r_v^2 - 1), (1 - \xi_v^0)(\xi_v^0/r_v^2 - 1))$, and $\mu_v = \mathbf{X}_{P_v}^T \mathbf{b}_v - \mathbf{X}_{\mathcal{T}_l \setminus v} \mathbf{a}_v + \mathbf{X}_{P_v} \mathbf{B}_{\mathcal{T}_l \setminus v}^T \mathbf{a}_v$, $\mu_v^D = \mathbf{X}_{P_v}^T \mathbf{b}_v - (\mathbf{X}\mathbf{D})_{\mathcal{T}_l \setminus v} \mathbf{a}_v + \mathbf{X}_{P_v} \mathbf{B}_{\mathcal{T}_l \setminus v}^T \mathbf{a}_v$. We then sample $U \sim \text{Unif}(0, 1)$ and set $\boldsymbol{\pi}^{s+1} = \boldsymbol{\pi}^*$ if $U \leq R$, and set $\boldsymbol{\pi}^{s+1} = \boldsymbol{\pi}^s$ otherwise.

To update undirected edges, given \mathbf{D} , let $\tilde{\mathbf{y}}_v = \mathbf{X}_v/d_v - \mathbf{X}_{P_v} \mathbf{b}_v$, and $\mathbf{x}_v = \mathbf{X}_{\mathcal{T}_l \setminus v} \mathbf{D}_{\mathcal{T}_l \setminus v} - \mathbf{X}_{P_v} \mathbf{B}_{\mathcal{T}_l \setminus v}^T$.

1. We first update the model selection parameters. Let s be the current state.

1.1. Add-delete or swap: with probability $1/2$, sample w_1 from $\mathcal{T}_l \setminus v$ and set $\eta_{vw_1}^* = \eta_{w_1 v}^* = 1 - \eta_{vw_1}^s$. Else, sample w_2 from $\{w : \eta_{vw} = 0\} \setminus \{v\}$, w_3 from $\{w : \eta_{vw} = 1\}$ and set $\eta_{vw_2}^* = \eta_{w_2 v} = 1$ and $\eta_{vw_3} = \eta_{w_3 v} = 0$.

1.2. Compute the acceptance ratio:

add/delete: $R = \prod_{r \in \{v, w_1\}} \frac{f(\tilde{\mathbf{y}}_r | \mathbf{x}_r, \boldsymbol{\eta}_r^*, k_{rr}) p(\boldsymbol{\eta}_r^*)}{f(\tilde{\mathbf{y}}_r | \mathbf{x}_r, \boldsymbol{\eta}_r^s, k_{rr}) p(\boldsymbol{\eta}_r^s)}$,

swap: $R = \prod_{r \in \{v, w_2, w_3\}} \frac{f(\tilde{\mathbf{y}}_r | \mathbf{x}_r, \boldsymbol{\eta}_r^*, k_{rr}) p(\boldsymbol{\eta}_r^*)}{f(\tilde{\mathbf{y}}_r | \mathbf{x}_r, \boldsymbol{\eta}_r^s, k_{rr}) p(\boldsymbol{\eta}_r^s)}$,

where $f(\tilde{\mathbf{y}}_v | \mathbf{x}_v, \boldsymbol{\eta}_v, k_{vv})$ is the density function of a normal distribution with mean 0 and variance

$$\frac{1}{k_{vv}} (\mathbf{I} - \mathbf{x}_v^\eta (\mathbf{x}_v^{\eta T} \mathbf{x}_v^\eta + \mathbf{G}_v^{-1})^{-1} \mathbf{x}_v^{\eta T})^{-1},$$

for $\mathbf{G}_v = \mathbf{I}/\lambda_l$ and $p(\boldsymbol{\eta}_r) = \prod_{k \in C(r)} p_{rk}^{\eta_r k} (1 - p_{rk})^{1 - \eta_r k}$.

1.3. Sample $U \sim \text{Unif}(0, 1)$ and set $\boldsymbol{\varepsilon}^{s+1} = \boldsymbol{\varepsilon}^*$ if $U \leq R$, and set $\boldsymbol{\varepsilon}^{s+1} = \boldsymbol{\varepsilon}^s$ otherwise.

2. Gibbs sampling for \mathbf{a}_v : for all r in $\{v, w_1\}$ or $\{v, w_2, w_3\}$,

$$\mathbf{a}_r | \tilde{\mathbf{y}}_r, \tilde{\mathbf{x}}_r, \boldsymbol{\eta}_r, k_{rr} \sim N \left((\mathbf{x}_r^{\eta T} \mathbf{x}_r^\eta + \mathbf{G}_r^{-1})^{-1} \mathbf{x}_r^{\eta T} \tilde{\mathbf{y}}_r, \frac{1}{k_{rr}} (\mathbf{x}_r^{\eta T} \mathbf{x}_r^\eta + \mathbf{G}_r^{-1})^{-1} \right). \quad (\text{S.13})$$

3. Gibbs sampling for k_{rr} : for all r in $\{v, w_1\}$ or $\{v, w_2, w_3\}$,

$$p(k_{rr} | \tilde{\mathbf{x}}_r, \mathbf{x}_r, \boldsymbol{\eta}_r, \mathbf{a}_r) = \text{Gamma}(A_1, A_2), \quad (\text{S.14})$$

where

$$\begin{aligned} A_1 &= \frac{n + \delta_l + |\mathcal{T}_l| - 1 + \|\boldsymbol{\eta}_r\|_0}{2}, \\ A_2 &= \frac{\lambda_l}{2} + \frac{1}{2} [(\tilde{\mathbf{y}}_r - \mathbf{x}_r^\eta \mathbf{a}_r^\eta)^T (\tilde{\mathbf{y}}_r - \mathbf{x}_r^\eta \mathbf{a}_r^\eta) + \mathbf{b}_r^{\gamma T} (\mathbf{I}/\lambda_l)^{-1} \mathbf{b}_r^\gamma \\ &\quad + (\lambda_l + |\mathcal{T}_l| - 1) \mathbf{a}_r^{\eta T} \mathbf{a}_r^\eta], \end{aligned}$$

and $\|\cdot\|_0$ denotes the number of nonzero elements in the vector.

To update directed edges between layers, let G be the current graph and u_1, u_2, \dots be vertices in the neighbor set of v in G . Set $\tilde{\mathbf{y}}_v = X_v/d_v - \boldsymbol{\varepsilon}_{\mathcal{T}_l \setminus v}^T \mathbf{a}_v$, $\tilde{\mathbf{x}}_v = \mathbf{D}_{[1:l-1]} \mathbf{X}_{[1:l-1]}$.

1. Metropolis-Hastings for edge selection: let s be the current state.

1.1. Add-delete or swap: with probability $1/2$, sample k_1 from $\mathbf{X}_{[1:l-1]}$ and set $\gamma_{vk_1}^* = 1 - \gamma_{vk_1}^s$. Otherwise sample k_2 from the parent nodes of v , k_3 from the set of nodes in $[1 : l - 1]$ that are not connected to v , and set $\gamma_{vk_2}^* = 0$ and $\gamma_{vk_3} = 1$.

1.2. Compute the acceptance ratio:

$$R = \frac{f(\tilde{\mathbf{y}}_v | \tilde{\mathbf{x}}_v, \boldsymbol{\gamma}^*, k_{vv})p(\boldsymbol{\gamma}^*)}{f(\tilde{\mathbf{y}}_v | \tilde{\mathbf{x}}_v, \boldsymbol{\gamma}^s, k_{vv})p(\boldsymbol{\gamma}^s)},$$

where $f(\tilde{\mathbf{y}}_v | \tilde{\mathbf{x}}_v, \boldsymbol{\gamma}, k_{vv})$ is the density function of normal distribution with mean 0 and variance

$$\frac{1}{k_{vv}} (\mathbf{I} - \mathbf{x}_v^\gamma (\mathbf{x}_v^{\gamma T} \mathbf{x}_v^\gamma + \mathbf{G}_v^{-1})^{-1} \mathbf{x}_v^\gamma)^{-1},$$

for $\mathbf{G}_v = \mathbf{I}/\lambda_l$ and $p(\boldsymbol{\gamma}) = \prod_{v \in \mathcal{T}_l, w \in \mathcal{T}_{[1:l-1]}} q_{vw}^{\gamma_{vw}} (1 - q_{vw})^{1 - \gamma_{vw}}$.

1.3. Sample $U \sim \text{Unif}(0, 1)$ and set $\boldsymbol{\gamma}^{s+1} = \boldsymbol{\gamma}^*$ if $U \leq R$, and set $\boldsymbol{\gamma}^{s+1} = \boldsymbol{\gamma}^s$ otherwise.

2. Gibbs sampling for \mathbf{b}_v :

$$\mathbf{b}_v | \tilde{\mathbf{y}}_v, \tilde{\mathbf{x}}_v, \boldsymbol{\gamma}_v, k_{vv} \sim N \left((\mathbf{x}_v^{\gamma T} \mathbf{x}_v^\gamma + \mathbf{G}_v^{-1})^{-1} \mathbf{x}_v^{\gamma T} \tilde{\mathbf{y}}_v, \frac{1}{k_{vv}} (\mathbf{x}_v^{\gamma T} \mathbf{x}_v^\gamma + \mathbf{G}_v^{-1})^{-1} \right). \quad (\text{S.15})$$

3. Gibbs sampling for k_{vv} :

$$p(k_{vv} | \tilde{\mathbf{y}}_v, \tilde{\mathbf{x}}_v, \boldsymbol{\gamma}_v, \mathbf{b}_v) = \text{Gamma}(B_1, B_2), \quad (\text{S.16})$$

where

$$B_1 = \frac{n + \delta_l + |\mathcal{T}_l| - 1 + \|\boldsymbol{\gamma}_v\|_0}{2},$$

$$B_2 = \frac{\lambda_l}{2} + \frac{1}{2} [(\tilde{\mathbf{y}}_v - \mathbf{x}_v^{\gamma T} \mathbf{b}_v^\gamma)^T (\tilde{\mathbf{y}}_v - \mathbf{x}_v^{\gamma T} \mathbf{b}_v^\gamma) + \mathbf{b}_v^{\gamma T} (\mathbf{I}/\lambda_l)^{-1} \mathbf{b}_v^\gamma + (\lambda_l + |\mathcal{T}_l| - 1) \mathbf{b}_v^{\gamma T} \mathbf{b}_v^\gamma],$$

and $\|\cdot\|_0$ is the number of nonzero elements in the vector.

S.6 Additional Simulation Details

The most commonly used measure for the tail mass being heavier or lighter than that of the normal distribution is the kurtosis. A standardized kurtosis > 0 indicates heavier-than-normal tails. To analyze the performance of the three methods with respect to tail-heaviness measured by the kurtosis, we empirically calculate the kurtosis of a random variable following a mixture of normal and heavy-tailed distributions with the mixing factor being π . We perform this procedure for a range of π in $[0, 1]$. Based on these π values, we form the chain graph simulation datasets as described in Section 4 and evaluate the AUC values for 30 replications of data, for each of the three methods RCGM, BANS and LBBM. Figures S.2 – S.3 display the AUCs varying across different π and kurtosis levels respectively.

S.7 Pathway-wise Networks for Molecular-drug Interactions

We have pathway-level graphs obtained using RCGM for 10 key signaling pathways: apoptosis, cell cycle, DNA damage response, EMT, RAS/MAPK, RTK, PI3K/AKT, TSC/mTOR, core reactive and breast reactive. The graph for DNA damage response is displayed in Figure 5. The rest of the pathway graphs are displayed in Figures S.6 – S.14. For each graph,

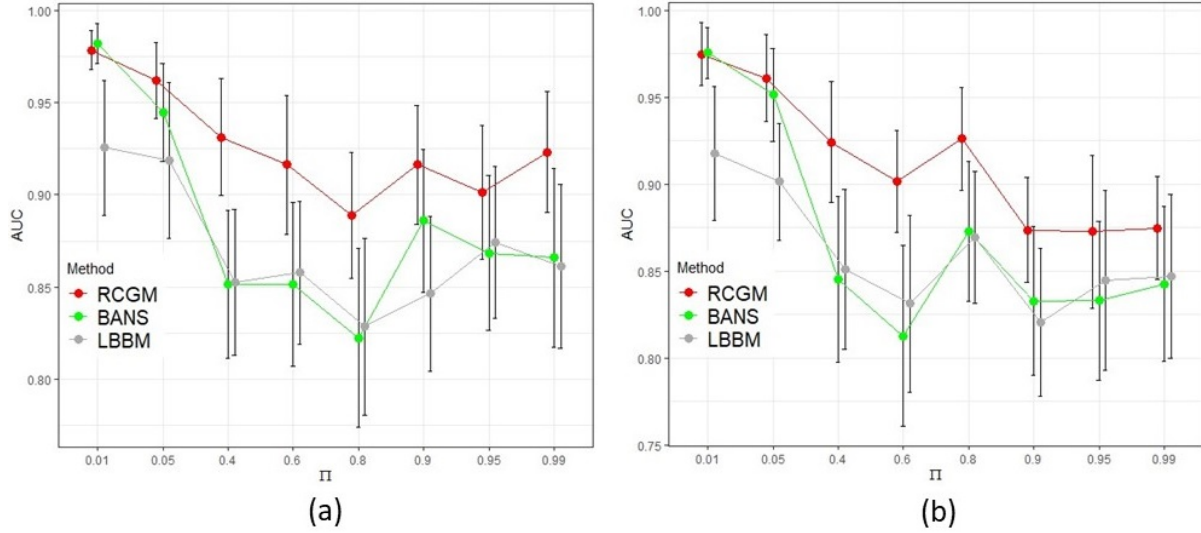


Figure S.2: Mean area under ROC curve across 30 replications for different levels of marginal tail-heaviness, measured by π . Interval of one standard deviation around each mean AUC is displayed through vertical lines. Panels (a) and (b) correspond to scaling by Exponential(mean = 2.5) and Inv-Gamma(shape = 3, rate = 6) respectively.

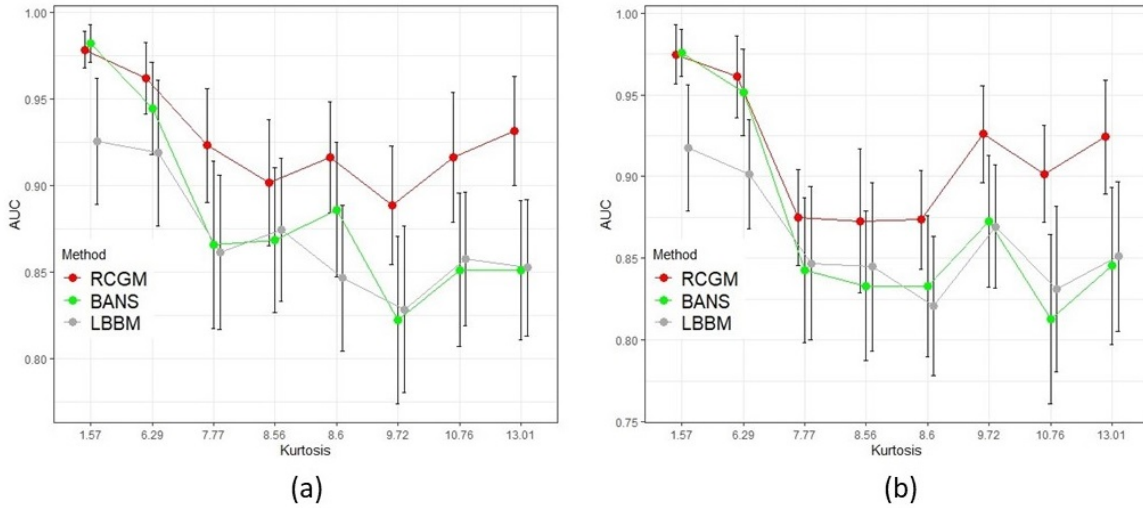


Figure S.3: Mean area under ROC curve across 30 replications for different levels of marginal tail-heaviness, measured by the kurtosis. Interval of one standard deviation around each mean AUC is displayed through vertical lines. Panels (a) and (b) correspond to scaling by Exponential(mean = 2.5) and Inv-Gamma(shape = 3, rate = 6) respectively.

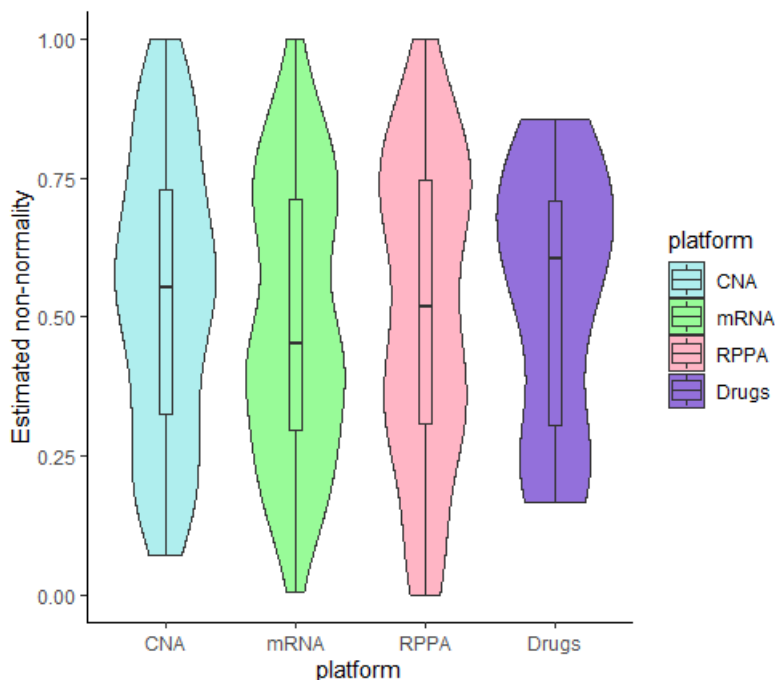


Figure S.4: Violin plot of the estimated node-wise non-normality $\hat{\pi}_v$ across all pathways.

the edge width is proportional to the posterior edge inclusion probability obtained from MCMC samples. The platform-wise violin plot of the estimated non-normality scores π_v are displayed in Figure S.4.

We display the between-drug edges detected across pathways in Figure S.5. Two clusters of drugs emerge from this analysis - the first cluster consisting of icotinib, vinorelbine, paclitaxel, osimertinib, gemcitabine and carboplatin, and the second cluster including afatinib, brigatinib, etoposide, sorafenib, alectinib, docetaxel and erlotinib. Dependencies of icotinib with vinorelbine, paclitaxel and osimertinib and those of afatinib with sorafenib, etoposide and brigatinib were detected in all 10 pathways. Strong dependencies between drugs indicate that drugs' individual effects on cell viability after scaling for robustness and adjusting for effects of all other variables are strongly positively correlated.

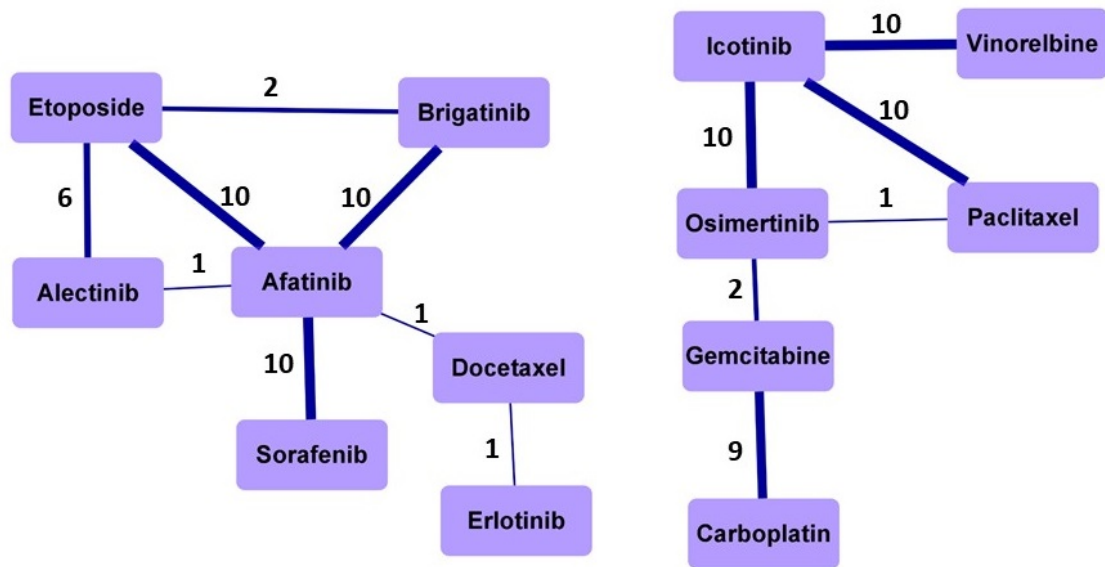


Figure S.5: Dependent drug pairs captured across the 10 pathways. Each edge width is proportional to, and marked with the number of pathways (out of 10) the corresponding drug-drug dependency is detected in.

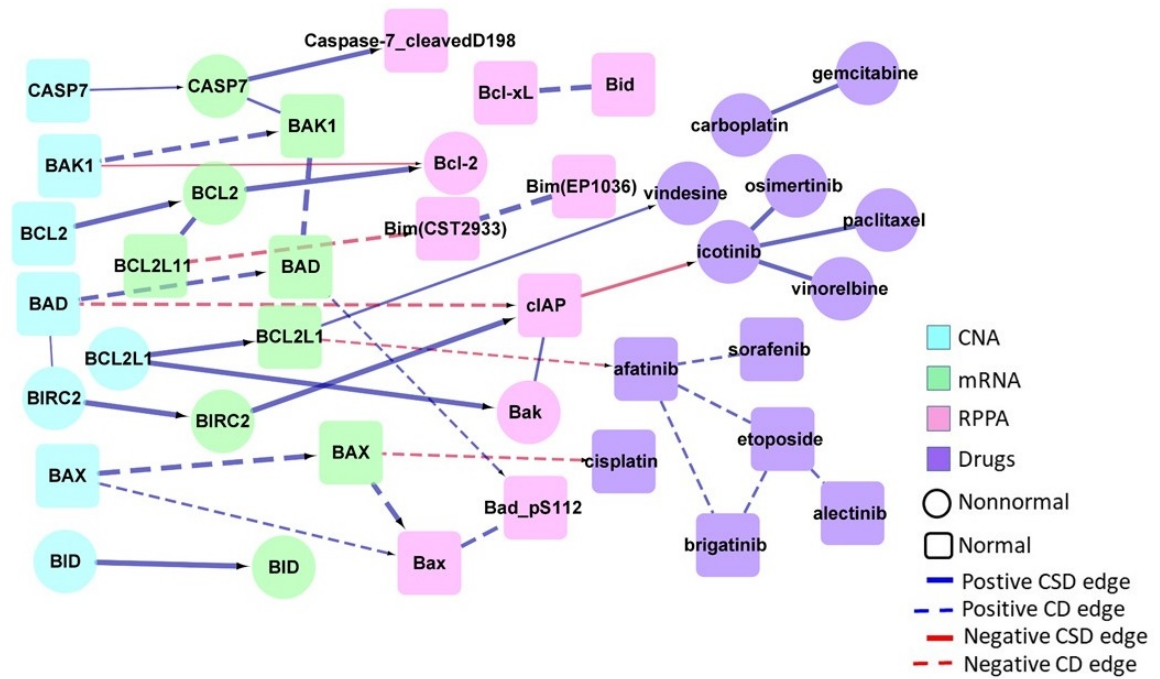


Figure S.6: The estimated multilayered network for the apoptosis pathway. Blue and red edges indicate positive and negative dependencies, while CD and CSD stand for conditionally dependent and conditionally sign-dependent edges respectively. The width of the edges is proportional to the posterior inclusion probabilities.

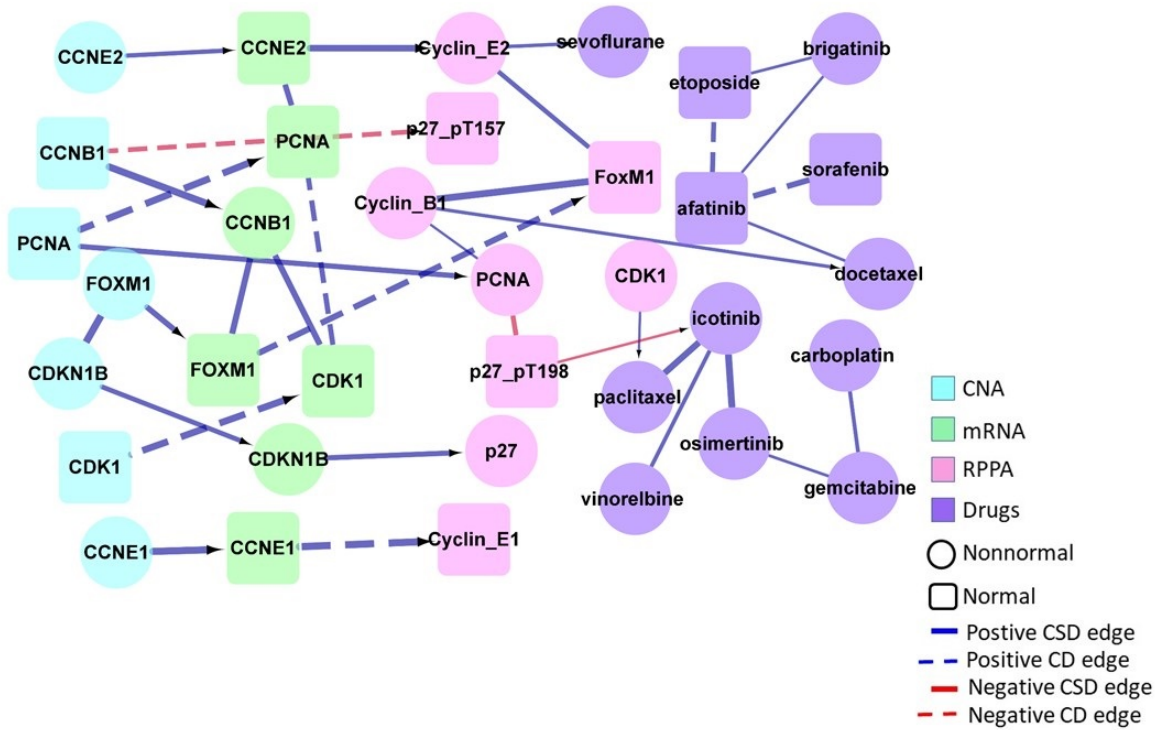


Figure S.7: The estimated multilayered network for the cell cycle pathway. Blue and red edges indicate positive and negative dependencies, while CD and CSD stand for conditionally dependent and conditionally sign-dependent edges respectively. The width of the edges is proportional to the posterior inclusion probabilities.

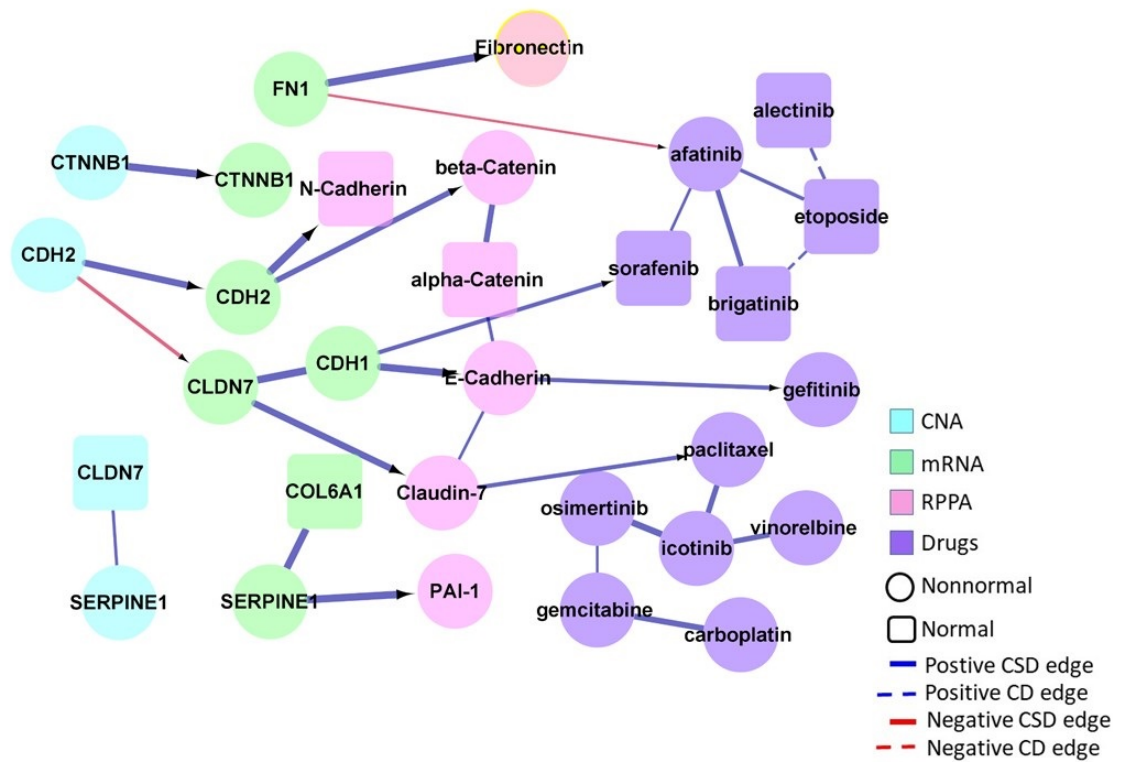


Figure S.8: The estimated multilayered network for the EMT pathway. Blue and red edges indicate positive and negative dependencies, while CD and CSD stand for conditionally dependent and conditionally sign-dependent edges respectively. The width of the edges is proportional to the posterior inclusion probabilities.

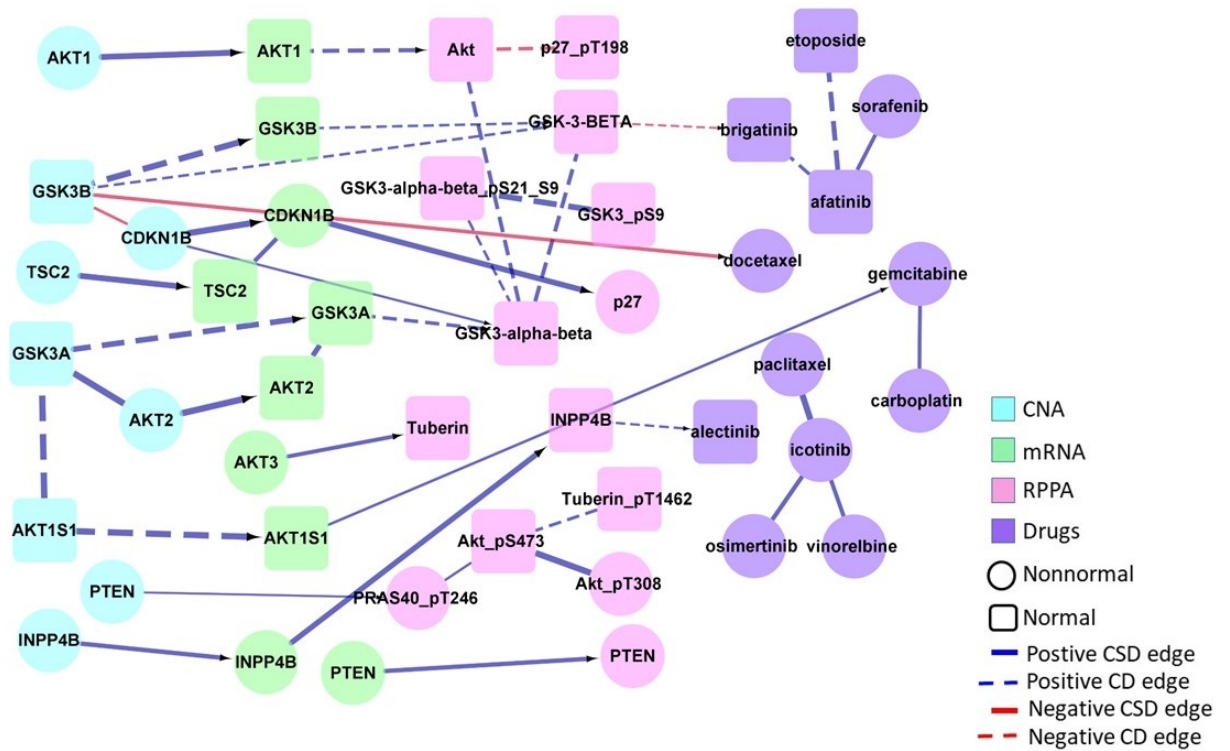


Figure S.9: The estimated multilayered network for the PI3K/AKT pathway. Blue and red edges indicate positive and negative dependencies, while CD and CSD stand for conditionally dependent and conditionally sign-dependent edges respectively. The width of the edges is proportional to the posterior inclusion probabilities.

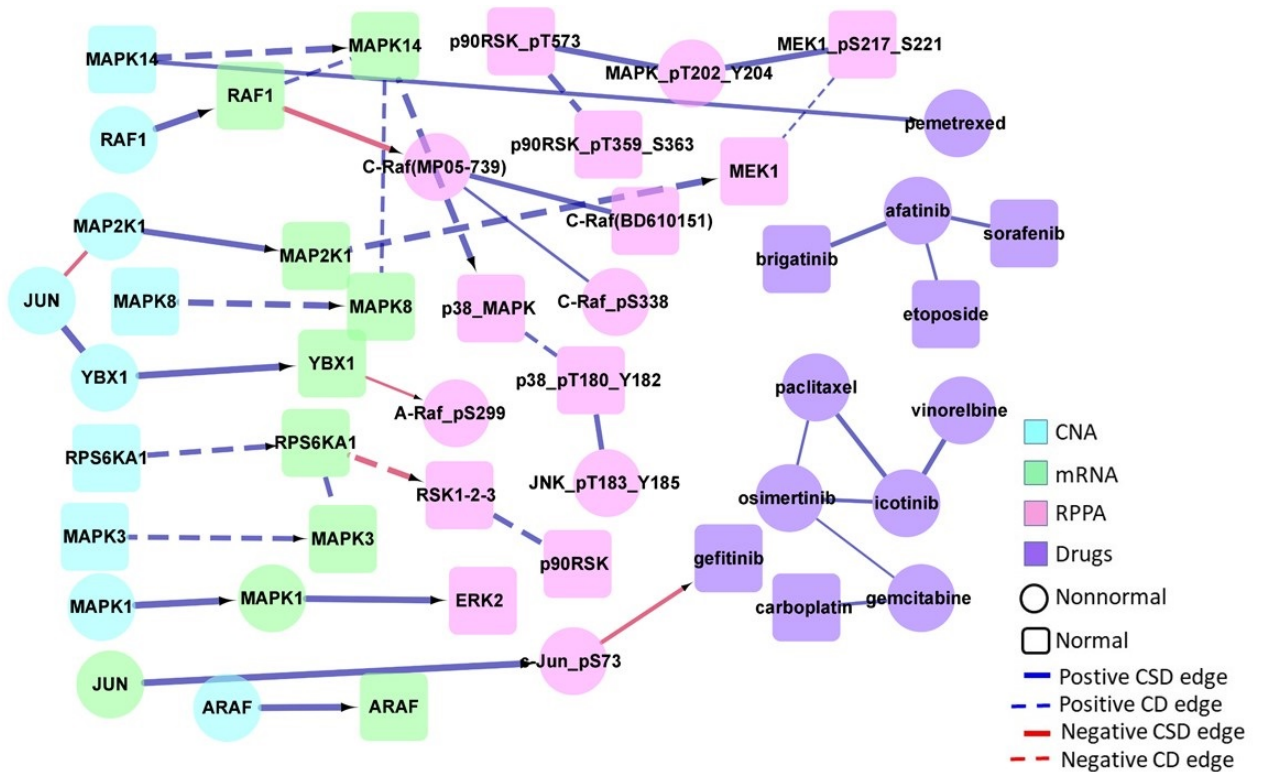


Figure S.10: The estimated multilayered network for the RAS/MAPK pathway. Blue and red edges indicate positive and negative dependencies, while CD and CSD stand for conditionally dependent and conditionally sign-dependent edges respectively. The width of the edges is proportional to the posterior inclusion probabilities.

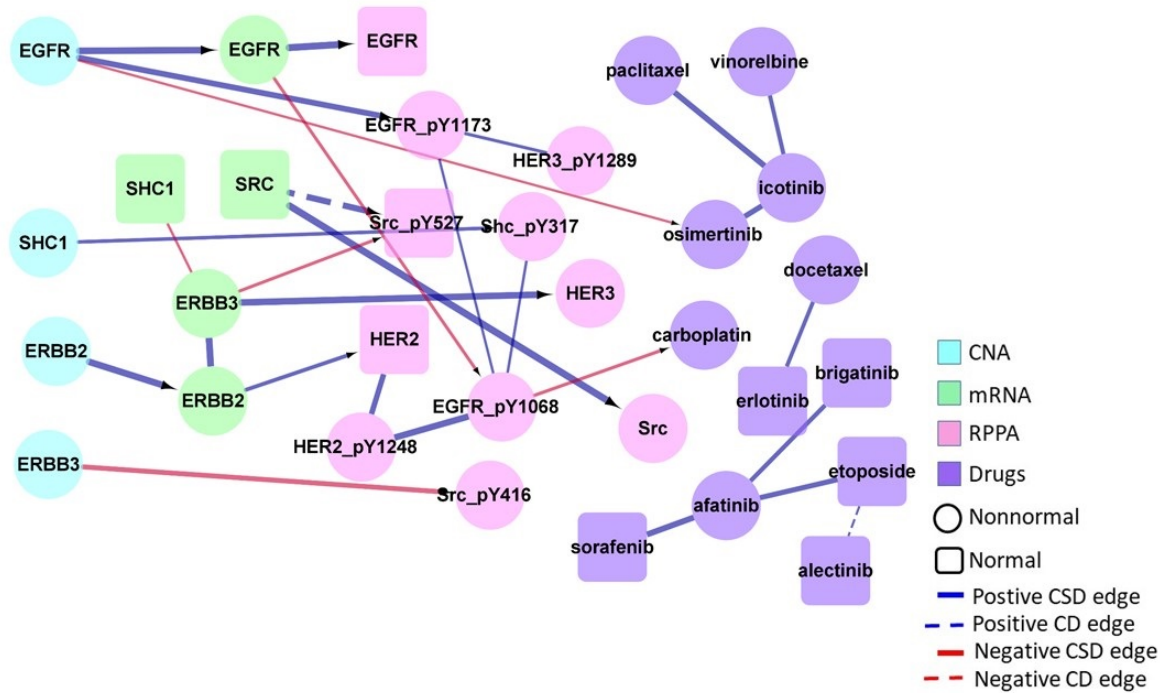


Figure S.11: The estimated multilayered network for the RTK pathway. Blue and red edges indicate positive and negative dependencies, while CD and CSD stand for conditionally dependent and conditionally sign-dependent edges respectively. The width of the edges is proportional to the posterior inclusion probabilities.

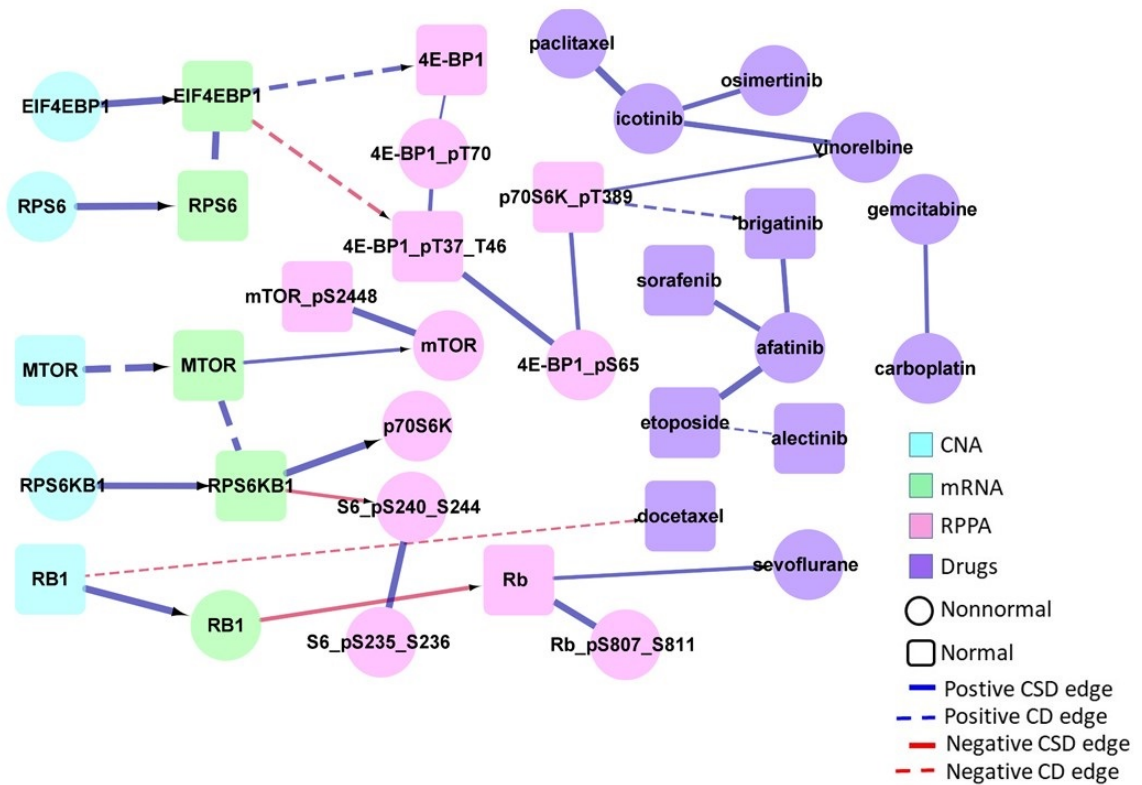


Figure S.12: The estimated multilayered network for the TSC/mTOR pathway. Blue and red edges indicate positive and negative dependencies, while CD and CSD stand for conditionally dependent and conditionally sign-dependent edges respectively. The width of the edges is proportional to the posterior inclusion probabilities.

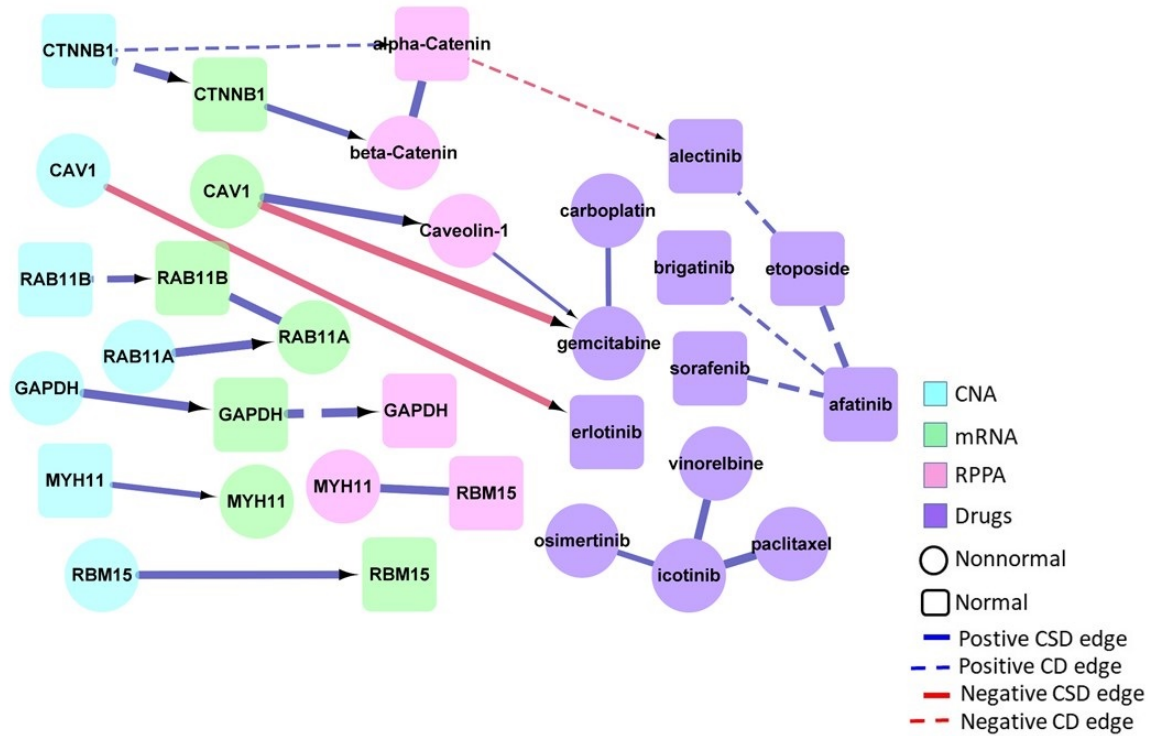


Figure S.13: The estimated multilayered network for the breast reactive pathway. Blue and red edges indicate positive and negative dependencies, while CD and CSD stand for conditionally dependent and conditionally sign-dependent edges respectively. The width of the edges is proportional to the posterior inclusion probabilities.

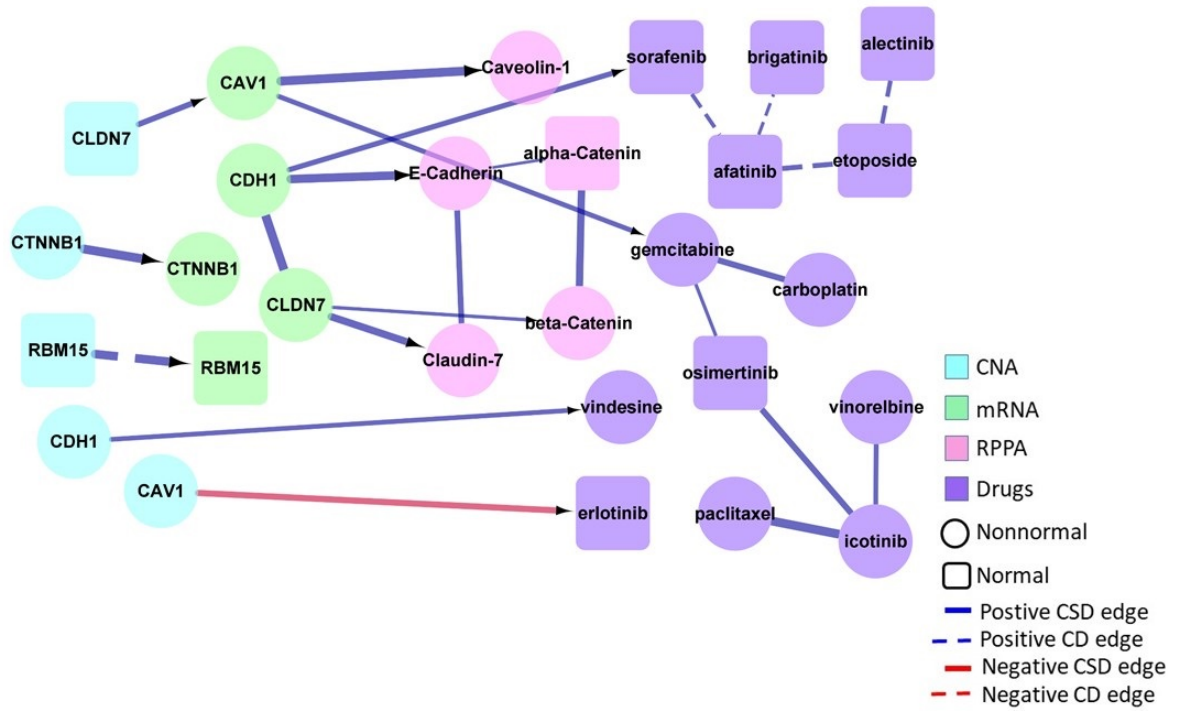
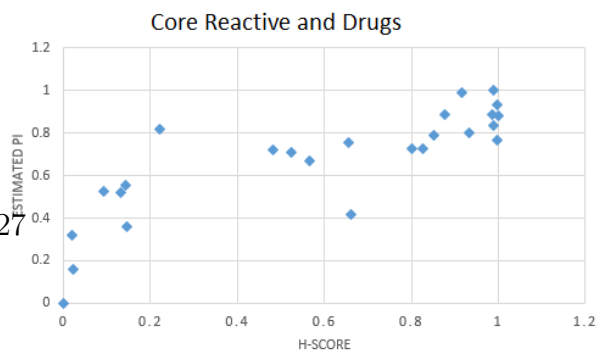
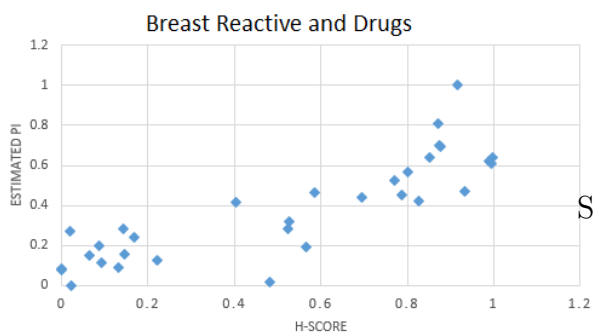
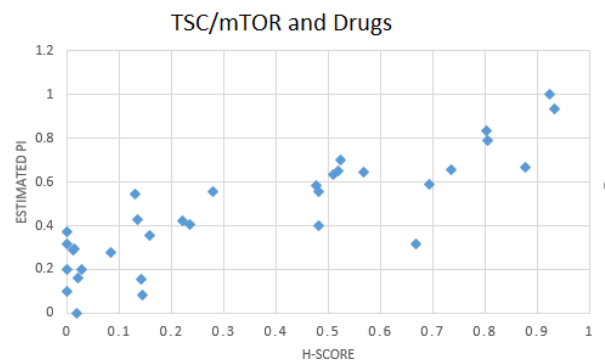
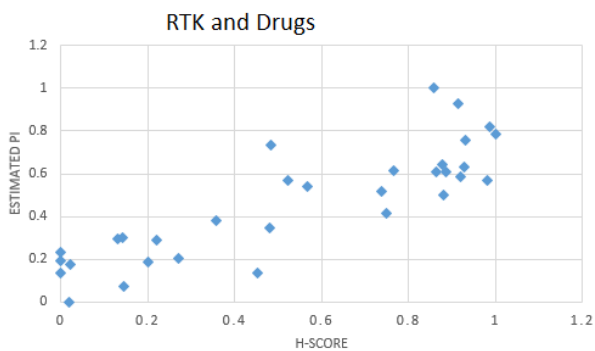
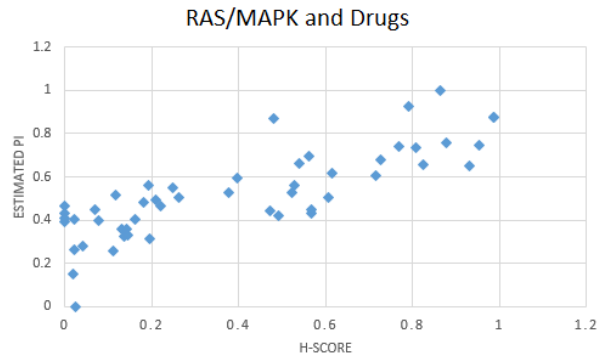
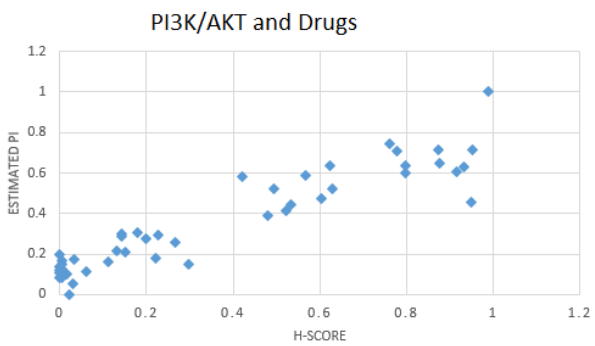
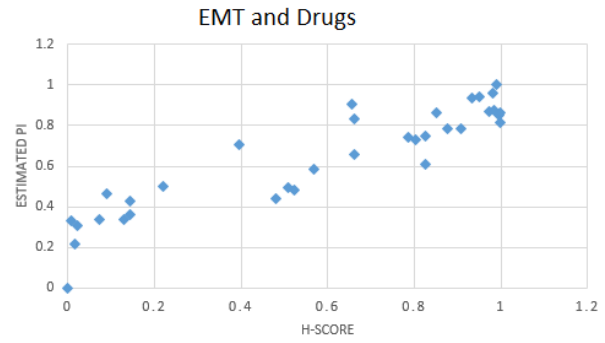
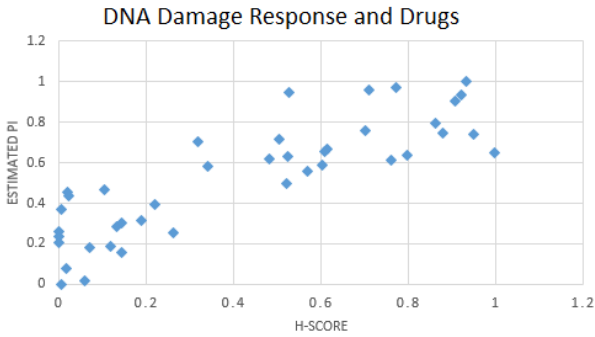
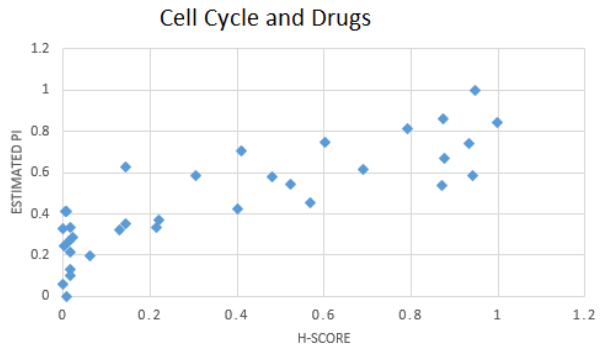
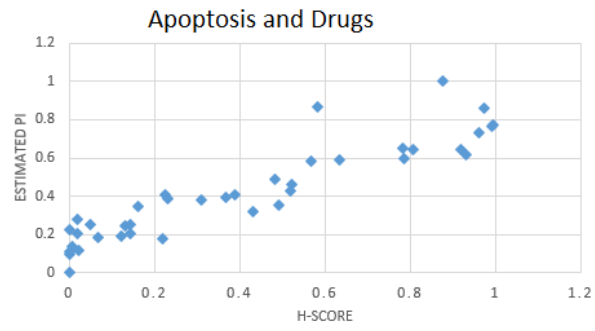


Figure S.14: The estimated multilayered network for the core reactive pathway. Blue and red edges indicate positive and negative dependencies, while CD and CSD stand for conditionally dependent and conditionally sign-dependent edges respectively. The width of the edges is proportional to the posterior inclusion probabilities.



S.27

Figure S.15: Pathway-wise H-score vs. $\hat{\pi}$

S.8 Supplementary Tables

We display the names of pathways chosen in our study along with the count of gene and protein memberships in each in Table S.1. The list of genes and proteins corresponding to each pathway is given in Table S.2. Tables S.3 – S.4 display the target genes, mechanism of action and primary diseases associated with the drugs used in our study.

Pathway	CNA	mRNA	RPPA
Apoptosis	9	9	10
Cell cycle	7	7	9
DNA damage response	10	10	13
EMT	7	7	9
PI3K/AKT	10	10	15
RAS/MAPK	10	10	19
RTK	5	5	11
TSC/mTOR	5	5	12
Breast reactive	7	7	7
Core reactive	5	5	7

Table S.1: Number of nodes in each platform of genomic information across 10 pathways.

Pathway	Gene	Antibodies
Apoptosis	BAD	Bad_pS112
Apoptosis	BAK1	Bak_Caution
Apoptosis	BAX	Bax
Apoptosis	BCL2	Bcl-2
Apoptosis	BCL2L1	Bcl-xL
Apoptosis	BID	Bid_Caution
Apoptosis	BCL2L11	Bim(CST2933), Bim(EP1036)
Apoptosis	CASP7	Caspase-7_cleavedD198_Caution
Apoptosis	BIRC2	cIAP_Caution
Cell cycle	CDK1	CDK1
Cell cycle	CCNB1	Cyclin_B1
Cell cycle	CCNE1	Cyclin_E1
Cell cycle	CCNE2	Cyclin_E2_Caution
Cell cycle	FOXM1	FoxM1
Cell cycle	CDKN1B	p27, p27_pT157_Caution, p27_pT198
Cell cycle	PCNA	PCNA_Caution
DNA damage response	TP53BP1	53BP1
DNA damage response	ATM	ATM
DNA damage response	BRCA2	BRCA2_Caution
DNA damage response	CHEK1	Chk1_Caution, Chk1_pS345_Caution
DNA damage response	CHEK2	Chk2, Chk2_pT68_Caution
DNA damage response	XRCC5	Ku80_Caution
DNA damage response	MRE11A	Mre11_Caution
DNA damage response	TP53	p53_Caution
DNA damage response	RAD50	RAD50
DNA damage response	RAD51	RAD51
DNA damage response	XRCC1	XRCC1_Caution
EMT	CTNNB1	alpha-Catenin, beta-Catenin, beta-Catenin_pT41_S45
EMT	CLDN7	Claudin-7
EMT	COL6A1	Collagen_VI
EMT	CDH1	E-Cadherin
EMT	FN1	Fibronectin
EMT	CDH2	N-Cadherin
EMT	SERPINE1	PAI-1

PI3K/AKT	AKT1	Akt, Akt_pS473, Akt_pT308
PI3K/AKT	AKT2	Akt, Akt_pS473, Akt_pT308
PI3K/AKT	AKT3	Akt, Akt_pS473, Akt_pT308
PI3K/AKT	GSK3B	GSK-3-beta_Caution, GSK3-alpha-beta, GSK3-alpha-beta_pS21_S9, GSK3_pS9
PI3K/AKT	GSK3A	GSK3_pS9, GSK3-alpha-beta, GSK3-alpha-beta_pS21_S9
PI3K/AKT	INPP4B	INPP4B
PI3K/AKT	CDKN1B	p27, p27_pT157_Caution, p27_pT198
PI3K/AKT	AKT1S1	PRAS40_pT246
PI3K/AKT	PTEN	PTEN
PI3K/AKT	TSC2	Tuberin, Tuberin_pT1462
RAS/MAPK	ARAF	A-Raf_pS299_Caution
RAS/MAPK	JUN	c-Jun_pS73
RAS/MAPK	RAF1	C-Raf(BD610151)_Caution, C-Raf(MP05-739), C-Raf_pS338
RAS/MAPK	MAPK1	ERK2_Caution, MAPK_pT202_Y204
RAS/MAPK	MAPK8	JNK_pT183_Y185
RAS/MAPK	MAPK3	MEK1
RAS/MAPK	MAP2K1	MEK1_pS217_S221, p38 alpha MAPK
RAS/MAPK	MAPK14	p38_MAPK, p38_pT180_Y182, p90RSK_Caution
RAS/MAPK	RPS6KA1	p90RSK_pT359_S363_Caution, p90RSK_pT573_Caution, RSK1-2-3_Caution, YB-1
RAS/MAPK	YBX1	c-Jun_pS73, C-Raf(BD610151)_Caution
RTK	EGFR	EGFR, EGFR_pY1068_Caution, EGFR_pY1173
RTK	ERBB2	HER2, HER2_pY1248_Caution
RTK	ERBB3	HER3, HER3_pY1289_Caution
RTK	SHC1	Shc_pY317
RTK	SRC	Src, Src_pY416_Caution, Src_pY527
TSC/mTOR	EIF4EBP1	4E-BP1, 4E-BP1_pS65, 4E-BP1_pT37_T46, 4E-BP1_pT70
TSC/mTOR	MTOR	mTOR, mTOR_pS2448_Caution
TSC/mTOR	RPS6KB1	p70S6K, p70S6K_pT389
TSC/mTOR	RB1	Rb_Caution, Rb_pS807_S811
TSC/mTOR	RPS6	S6_pS235_S236, S6_pS240_S244

Breast reactive	CTNNB1	alpha-Catenin, beta-Catenin, beta-Catenin_pT41_S45
Breast reactive	CAV1	Caveolin-1
Breast reactive	GAPDH	GAPDH_Caution
Breast reactive	MYH11	MYH11
Breast reactive	RBM15	RBM15
Core reactive	CTNNB1	alpha-Catenin, beta-Catenin, beta-Catenin_pT41_S45
Core reactive	CAV1	Caveolin-1
Core reactive	CLDN7	Claudin-7
Core reactive	CDH1	E-Cadherin
Core reactive	RBM15	RBM15

Table S.2: Antibodies and their target genes considered in RPPA analysis

Drug	Mechanism of Action	Target genes	Indication
Icotinib	EGFR inhibitor	EGFR	NSCLC
Osimertinib	EGFR inhibitor	EGFR	NSCLC
Gefitinib	EGFR inhibitor	EGFR	NSCLC
Afatinib	EGFR inhibitor	EGFR,ERBB2,ERBB4	NSCLC
Erlotinib	EGFR inhibitor	EGFR, NR1I2	NSCLC, pancreatic cancer
Brigatinib	EGFR inhibitor, ALK tyrosine kinase receptor inhibitor	ALK, EGFR	NSCLC
Alectinib	ALK tyrosine kinase receptor inhibitor	ALK, MET	NSCLC
Ceritinib	ALK tyrosine kinase receptor inhibitor	ALK, FLT3, IGF1R, INSR, TSSK1B	NSCLC
Crizotinib	ALK tyrosine kinase receptor inhibitor	ALK, MET	NSCLC
Paclitaxel	tubulin polymerization inhibitor	BCL2,MAP2,MAP4, MAPT,NR1I2,TLR4, TUBB,TUBB1	ovarian and breast cancer, NSCLC
Docetaxel	tubulin polymerization inhibitor	BCL2, MAP2, MAP4, MAPT,NR1I2, TUBB, TUBB1	NSCLC, breast and prostate cancer, gastric adenocarcinoma, HNSCC
Vindesine	tubulin polymerization inhibitor	TUBB, TUBB1	NSCLC,melanoma, breast cancer
Vinorelbine	tubulin polymerization inhibitor	TUBA1A, TUBA1B, TUBA1C, TUBA3C, TUBA3D, TUBA3E, TUBA4A, TUBB, TUBB1, TUBB2A, TUBB2B, TUBB3, TUBB4A, TUBB4B, TUBB6, TUBB8	NSCLC
Etoposide	topoisomerase inhibitor	TOP2A, TOP2B	NSCLC

Table S.3: List of drugs used in our analysis along with their targets.

Drug	Mechanism of action	Target genes	Indication
Pemetrexed	dihydrofolate reductase inhibitor, thymidylate synthase inhibitor	ATIC, DHFR, GART, TYMS	NSCLC, mesothelioma
Gemcitabine	ribonucleotide reductase inhibitor	CMPK1,RRM1,RRM2, TYMS	NSCLC,ovarian, breast and pancreatic cancer
Sevoflurane	membrane integrity inhibitor	ATP2C1, ATP5D, GABRA1, GABRA2, GABRA3, GABRA4, GABRA5, GABRA6, GABRB1, GABRB2, GABRB3, GABRD, GABRE, GABRG1, GABRG2, GABRG3, GABRP, GABRQ, GLRA1,GLRB,GRIA1, KCNA1, KCNK10, KCNK18,KCNK2, KCNK3, KCNK9,MT-ND1	anesthetic
Cisplatin	DNA synthesis inhibitor, DNA alkylating agent	XIAP	testicular carcinoma, ovarian and bladder cancer
Carboplatin	DNA alkylating agent, DNA inhibitor		ovarian cancer
Sorafenib	FLT3 inhibitor, KIT inhibitor, PDGFR tyrosine kinase receptor inhibitor, RAF inhibitor, RET tyrosine kinase inhibitor, VEGFR inhibitor	BRAF,DDR2,FGFR1, FLT3,FLT4,KDR,KIT, PDGFRB, RAF1, RET, FLT1	renal cell carcinoma (RCC), thyroid cancer, hepatocellular carcinoma (HCC)

Table S.4: List of drugs used in our analysis along with their targets.